Tellus (2001), 53B, 564–592
Printed in UK. All rights reserved

TELLUS
ISSN 0280–6509

Feedback mechanisms and sensitivities of ocean carbon uptake under global warming

By G.-K. PLATTNER*, F. JOOS, T. F. STOCKER and O. MARCHAL, *Climate and Environmental Physics, Physics Institute, University of Bern, Sidlerstrasse 5, Switzerland*

(Manuscript received 25 October 2000; in final form 9 April 2001)

ABSTRACT

Global warming simulations are performed with a coupled climate model of reduced complexity to investigate global warming–marine carbon cycle feedbacks. The model is forced by emissions of CO_2 and other greenhouse agents from scenarios recently developed by the Intergovernmental Panel on Climate Change and by CO_2 stabilization profiles. The uptake of atmospheric CO_2 by the ocean is reduced between 7 to 10% by year 2100 compared to simulations without global warming. The reduction is of similar size in the Southern Ocean and in low-latitude regions (32.5°S–32.5°N) until 2100, whereas low-latitude regions dominate on longer time scales. In the North Atlantic the CO_2 uptake is enhanced, unless the Atlantic thermohaline circulation completely collapses. At high latitudes, biologically mediated changes enhance ocean CO_2 uptake, whereas in low-latitude regions the situation is reversed. Different implementations of the marine biosphere yield a range of 5 to 16% for the total reduction in oceanic CO_2 uptake until year 2100. Modeled oceanic O_2 inventories are significantly reduced in global warming simulations. This suggests that the terrestrial carbon sink deduced from atmospheric O_2/N_2 observations is potentially overestimated if the oceanic loss of O_2 to the atmosphere is not considered.

1. Introduction

Increasing atmospheric concentrations of CO_2, non-CO_2 greenhouse gases (GHGs) and aerosols owing to emissions from combustion of fossil fuels, biomass burning and other anthropogenic sources, have the potential to induce substantial changes in the climate system in the near future (IPCC, 1996). To quantify possible consequences of an anthropogenic perturbation of the climate system, projections of future atmospheric CO_2, non-CO_2 GHGs and aerosols, based on scenarios of future GHG emissions (Legget et al., 1992; Nakićenović et al., 2000) are required. Such projections are affected by considerable uncertainties owing to a limited understanding of the mechanisms driving carbon sequestration by the ocean and the land biosphere (IPCC, 2001).

Ocean carbon storage is determined by a complex interplay between air–sea gas exchange, inorganic carbon chemistry, ocean circulation, and marine biology. Warming of ocean surface waters and changes in the hydrological cycle may stimulate different feedback mechanisms leading to a slowed uptake of anthropogenic carbon. For instance, an increase in sea-surface temperature (SST), would reduce the solubility of CO_2 in seawater and thus the oceanic uptake of CO_2. A reduction in the density of surface waters would lead to a reduction in deep-water formation (Manabe and Stouffer, 1993; Stocker and Schmittner, 1997) and transport to depth of excess carbon (Maier-Reimer et al., 1996; Sarmiento et al.,

* Corresponding author.
e-mail: plattner@climate.unite.ch

1998; Joos et al., 1999; Matear and Hirst, 1999). Changes in the biological cycling of organic material (OM) and calcite ($CaCO_3$) may alter the distributions of dissolved inorganic carbon (DIC) and alkalinity (ALK). Dilution/concentration effects at the ocean surface induced by changes in the hydrological cycle may alter surface DIC and ALK, thereby affecting surface-water CO_2 partial pressure (pCO_2) and the oceanic uptake of CO_2.

Previous studies investigated the oceanic uptake of anthropogenic carbon under constant climate (e.g., Revelle and Suess, 1957; Oeschger et al., 1975; Revelle, 1985; Maier-Reimer and Hasselmann, 1987; Sarmiento, 1991; Siegenthaler and Joos, 1992; Stocker et al., 1994; Murnane et al., 1999; Sarmiento et al., 2000; Orr et al., 2001). More recent studies considered the impact of global warming on ocean circulation, ocean carbon uptake (Klepper and de Haan, 1995; Maier-Reimer et al., 1996; Sarmiento and Le Quéré, 1996; Sarmiento et al., 1998; Joos et al., 1999; Matear and Hirst, 1999), and on atmospheric CO_2 (Maier-Reimer et al., 1996; Joos et al., 1999; Cox et al., 2000; Lenton, 2000; Friedlingstein et al., 2001). These studies found that the CO_2 uptake by the ocean is reduced between 4 to 28% during the 21st century in simulations with global warming compared to simulations without it. The geographical distribution of the reduction in CO_2 uptake by the ocean and the strength of individual feedback processes differ widely between the various studies.

In an earlier study (Joos et al., 1999), we forced a prognostic version of a zonally averaged physical-biogeochemical climate model (Marchal et al., 1998a) with (1) IS92 GHG emission scenarios (Legget et al., 1992) and (2) profiles that lead to a stabilization of atmospheric CO_2 (Wigley et al., 1997). We found that in all global warming simulations, the Atlantic thermohaline circulation (THC) weakens by 30 to 60% by year 2100. The projected atmospheric CO_2 was around 4% higher in simulations with global warming than in simulations without it. The CO_2 uptake by the ocean was reduced by 8 to 10% for this century, owing mainly to lowered CO_2 solubility caused by increasing SST. In simulations where the formation of North Atlantic Deep Water (NADW) stops completely after year 2100, the uptake was reduced by 27% until year 2500, mainly caused by the slow-down of the surface-to-deep mixing. Overall, changes in ocean carbon uptake as reported by Joos et al. (1999) are in the range of recent studies using three-dimensional Ocean General Circulation Models (OGCMs) (Maier-Reimer et al., 1996; Sarmiento and Le Quéré, 1996; Sarmiento et al., 1998; Matear and Hirst, 1999).

In this paper, we extend the global analysis by Joos et al. (1999) using the same climate model of reduced complexity. The purpose of this study is (1) to evaluate in detail different feedback mechanisms contributing to the changes in ocean carbon uptake and to study their spatial distribution; (2) to investigate global warming feedbacks for the non-intervention GHG emission scenarios developed recently by the writing team of the Special Report on Emission Scenarios (SRES) of the Intergovernmental Panel on Climate Change (IPCC) (Nakićenović et al., 2000); and (3) to analyze changes in the distribution of carbon-related oceanic tracers such as phosphate (PO_4) and dissolved oxygen (O_2). We also discuss implications of a potential oceanic O_2 loss to the atmosphere for the interpretation of atmospheric O_2/N_2 observations.

The paper is organized as follows. In Section 2, we briefly present the zonally averaged climate model and the standard experimental setup, the IPCC non-intervention SRES emission scenarios (Nakićenović et al., 2000), and the WRE CO_2 stabilization profiles (Schimel et al., 1997; Wigley et al., 1997). In Section 3, we introduce various global warming–marine carbon cycle feedback mechanisms associated with the CO_2 uptake by the ocean. In Section 4, results from several global warming simulations are discussed. Tracer distributions at year 2100 of warming simulations are compared to steady state distributions and to distributions obtained assuming constant climate. The feedback mechanisms contributing to changes in the uptake of atmospheric CO_2 by the ocean are quantified. In Section 5, we discuss results from OGCM studies and compare these results to our findings. Conclusions follow in Section 6.

2. Model and methods

The climate model includes components describing (1) the physical climate system, (2) the cycling of carbon and related elements, and (3) a

module to calculate concentrations of non-CO_2 GHGs and radiative forcing by atmospheric CO_2, non-CO_2 GHGs and aerosols. The physical and biogeochemical parameters of the model are set as in Joos et al. (1999) and listed in Table 1.

The model has been extensively used for paleoclimatic studies (Marchal et al., 1998b; Marchal et al., 1999a) and results are broadly consistent with those from comprehensive OGCMs. The modeled ocean uptake and the oceanic distribution of chlorofluorocarbons are in good agreement with observations and with results from OGCMs (Dutay et al., 2001). For GHG forcing, the model has a transient response of NADW formation and meridional heat transport (Stocker and Schmittner, 1997; Schmittner and Stocker, 1999; Joos et al., 1999) that is in agreement with that of the Geophysical Fluid Dynamics Laboratory (GFDL) coupled ocean–atmosphere general circulation model (Manabe and Stouffer, 1994) and that lies within the range of current coupled climate models (Cubasch et al., 2001). The sensitivity of Southern Ocean deep-water formation to global warming (Schmittner and Stocker, 1999) is smaller than found for comprehensive OGCMs (Sarmiento et al., 1998; Matear and Hirst, 1999). The model's average ocean carbon uptake for 1980–1989 and 1990–1999 is 2.0 and 2.3 GtC yr^{-1}, respectively, consistent with most recent results obtained with OGCMs (Schimel et al., 1996; Orr et al., 2001) and close to data-based estimates (Keeling et al., 1996; Gruber, 1998; Sabine et al., 1999; Battle et al., 2000; Gruber and Keeling, 2001).

Next, we provide a brief description of the climate model. Further details can be found in Marchal et al. (1998a), Marchal et al. (1998b), and Schmittner and Stocker (1999).

2.1. Model components

The ocean physical component is the zonally averaged, 3-basin circulation model of Stocker et al. (1992), with the dynamical closure scheme described by Wright et al. (1995). The basin geometry and spatial grid are as in Stocker and Wright (1996), with the Atlantic, Indian and Pacific basins represented individually and connected by a zonally well-mixed Antarctic circumpolar basin (Southern Ocean). A flat bottom

Table 1. *Physical and biogeochemical parameters of the climate model*

Model parameters	Standard setup	Range
Ocean circulation model		
vertical eddy diffusivity ($m^2\,s^{-1}$)	$0.4 \cdot 10^{-4}$	0.2–0.6
horizontal eddy diffusivity ($m^2\,s^{-1}$)	1000	
sea-ice formation rate in Southern Ocean, q_{SO} (Sv)	0.5	
water volume for plume generation in Antarctica, V_{SO} (Sv)	50	
restoring surface salinity at 72.5°N in Atlantic (psu)[a]	34.9	
Ocean biogeochemical model		
restoring time for PO_4 in euphotic zone (d)	100	
fraction of export production going into DOC_l (1)	0.5	0.25–0.75
ocean mean content of DOC_l ($mmol\,m^{-3}$)	10	5–20
ocean maximum $CaCO_3$/C production ratio ($mol\,mol^{-1}$)	0.1	0.05–0.2
length scale for $CaCO_3$ dissolution (m)	3000	
air–sea CO_2 transfer coefficient ($mmol\,m^{-2}\,yr^{-1}\,\mu atm^{-1}$) (Broecker et al., 1985)	67	
exponent in fast-sinking POC remineralization profile (1) (Bishop, 1989)	0.858	
decay rate of DOC_l (yr^{-1}) (Najjar et al., 1992)	variable	
depth of the euphotic zone (m)	100	
Terrestrial biosphere model		
fertilization factor β (1) (Joos et al., 1996)	0.287	

The standard physical and biogeochemical parameters are set as in Joos et al. (1999). For parameters varied in sensitivity tests the applied range is given additionally.
[a]Surface salinity is allowed to evolve freely during global warming simulations.

topography is specified. The governing equations are written in spherical coordinates and include hydrostatic, Boussinesq and rigid-lid approximations. Momentum equations are balances between Coriolis forces, horizontal pressure gradients and zonal wind stress. The lateral subgrid-scale mixing is horizontal and vertical and horizontal eddy diffusivities are constant. In the region around Antarctica we parameterize the effect of brine rejection due to seasonally varying sea-ice cover, because the seasonal cycle is neglected in the model. The salt ejected during sea-ice formation, prescribed at a rate of q_{SO}, is mixed with a specified volume of surface water, V_{SO}, and slotted into the water column at its stability level to mimick newly formed deep water flowing down canyons with small entrainment. The usual convection scheme based on instantaneous mixing is applied thereafter. A more detailed description can be found in Stocker and Wright (1996). The ocean model is coupled to a zonally and vertically averaged Energy Balance Model (EBM) of the atmosphere (Stocker et al., 1992) including an "active" hydrological cycle (Schmittner and Stocker, 1999).

The ocean biogeochemical component is a simple description of the cycles of carbon, carbon isotopes, O_2, and carbon-related tracers (Marchal et al., 1998a). The tracers considered are phosphate (PO_4), which is taken as the biolimiting nutrient, dissolved inorganic carbon (DIC), alkalinity (ALK), labile dissolved organic carbon (DOC_l), dissolved oxygen (O_2), and ^{13}C and ^{14}C in DIC and in DOC_l. Salinity-normalized tracer concentrations are transported in the model. This avoids the need for an explicit formulation of the effect of surface freshwater fluxes in the tracer continuity equation. A prognostic description of export production is applied, to account for changes in the ocean carbon cycle and atmospheric CO_2 driven by changes in ocean circulation. River input and sediment burial are omitted, i.e., all the organic carbon and calcite ($CaCO_3$) produced in the euphotic zone (top 100 m) are entirely recycled in the water column below. The net local consumption of organic carbon (J_{org}) is related to the PO_4 availability via Michaelis–Menten kinetics:

$$J_{org} = J_{pot} \frac{PO_4}{K_{PO_4} + PO_4}, \quad (1)$$

where J_{pot} is a potential consumption rate diagnosed from the spin-up and K_{PO_4} is a half saturation constant for PO_4 uptake (Marchal et al., 1998b). The local $CaCO_3$ production is scaled to J_{org} by a temperature-dependent production ratio. The ratio between the production of $CaCO_3$ and the production of organic material (OM) increases with temperature to reach a prescribed maximum in warm surface waters (Table 1) (Drange, 1994). We assume temporally and spatially constant stoichiometric ratios between biogenic fluxes. Export production is evenly partitioned between fast sinking particulate organic carbon and DOC_l, both remineralized below the euphotic zone. The air–sea gas exchange of carbon is calculated using a constant air–sea CO_2 transfer coefficient.

The model is complemented by a simple 4-box representation of the terrestrial biosphere (Siegenthaler and Oeschger, 1987), to account to first order for changes in terrestrial carbon storage under rising CO_2 and for the exchange of carbon isotopes between the atmosphere and the biosphere. Net primary production depends logarithmically on atmospheric CO_2 (Joos et al., 1996; Kicklighter et al., 1999). The terrestrial biota model is tuned to match estimates of the terrestrial carbon sink during the 1980's (Schimel et al., 1996) and the terrestrial CO_2 uptake simulated for future scenarios is well within the range obtained with current spatially resolved models (Kicklighter et al., 1999; Prentice et al., 2001). We emphasize that the impact of global warming on terrestrial carbon storage (Cao and Woodward, 1998; Meyer et al., 1999; Cox et al., 2000; Lenton, 2000; Friedlingstein et al., 2001) is not considered in this study. The ocean and the land biota exchange CO_2, ^{13}C and ^{14}C via the well-mixed atmosphere.

Finally, the module designed to calculate radiative forcing by atmospheric, CO_2 non-CO_2 GHGs and aerosols, is based on work summarized in Fuglestvedt and Berntsen (1999). The implementation of radiative forcing used here differs slightly from that in previous studies (Stocker and Schmittner, 1997; Schmittner and Stocker, 1999; Joos et al., 1999). We include the additional forcing owing to radiative forcing by CO_2, non-CO_2 GHGs and aerosols and to temperature-dependent feedbacks related to changes in atmospheric water vapor as (R. Knutti, personal communication):

$$\Delta F(t) = \Delta F_{2x} \log\left(\frac{CO_{2,eq}(t)}{CO_{2,eq}(0)}\right)\frac{1}{\log 2} + \lambda(T(t) - T(0)), \quad (2)$$

where the radiative forcing is expressed in units of equivalents of CO_2 ($CO_{2,eq}$). The radiative forcing for a doubling of $CO_{2,eq}$, is given by $\Delta F_{2x} = 3.71$ W m^{-2} (Myhre et al., 1998). $CO_{2,eq}(0)$ and $CO_{2,eq}(t)$ are the preindustrial and the actual atmospheric $CO_{2,eq}$ concentrations, and $T(t) - T(0)$ denotes the change in global-mean air temperature since preindustrial times. The inclusion of a temperature-dependent feedback term related to changes in atmospheric water vapor results in a retarded response of air temperature and NADW formation compared to previous global warming simulations (Stocker and Schmittner, 1997; Schmittner and Stocker, 1999; Joos et al., 1999). As a consequence, the reduction in uptake of atmospheric CO_2 by the ocean due to global warming is damped and delayed when using eq. (2). In contrast, the global-mean atmospheric temperature increase at equilibrium remains unchanged for a given climate sensitivity, ΔT_{2x}. To obtain a climate sensitivity of the EBM of 3.7°C in the standard global warming simulations, the feedback parameter λ is set to 2.18 W m^{-2} K^{-1}. For the constant-climate baseline simulation ΔT_{2x} is set to 0°C.

2.2. Standard model setup

The standard model spin-up is a multi-step procedure. First, the ocean model is spun up from rest for 11,000 years by relaxing the surface values of temperature and salinity to the zonal and annual mean climatological data of Levitus (1982) with a restoring time scale of 50 days. Zonal and annual mean wind stress based on the climatology of Han and Lee (1983) is applied at the ocean surface. The ocean biogeochemical component is then in a diagnostic mode, where euphotic zone PO_4 values are restored towards observations (Conkright et al., 1994) with a restoring time scale of 100 days. Preindustrial atmospheric CO_2 and $\delta^{13}C$ are prescribed to 277.97 ppm and -6.4‰, respectively. Second, the ocean model is forced by surface freshwater fluxes diagnosed from the previous integration while surface temperatures are still restored towards the climatological data. The terrestrial biosphere is coupled and the model is further integrated for 1000 years. Atmospheric CO_2 and $\delta^{13}C$ are allowed to evolve freely according to the exchanges with the ocean surface and the terrestrial biosphere. Third, the atmospheric EBM is coupled and the climate model is integrated for another 7000 years. At the end of this step we diagnose the steady state value of J_{pot} from PO_4 and J_{org} in the euphotic zone (Marchal et al., 1998b). This value is then used in the final step of the spin-up to describe J_{org} as a function of PO_4 availability in the euphotic zone (eq. (1)). The climate model is integrated for an additional 1000 years in this prognostic mode. All tracer fields are virtually unchanged after the first step. The globally averaged sea-to-air flux of CO_2 is about $2 \cdot 10^{-7}$ GtC yr^{-1} in the modeled preindustrial steady state.

We compare key model results for preindustrial times to observational estimates. The model reasonably reproduces the main features of the modern large-scale global ocean circulation, with deep-water formation in the North Atlantic and the Southern Ocean (Schmittner and Stocker, 1999). Modeled formation of NADW is 25 Sv at preindustrial times. This value is higher, but still consistent with most recent estimates of 15 ± 2 Sv derived from hydrographic data reported by Ganachaud and Wunsch (2000) and with estimates of 15 to 20 Sv reported by Gordon (1986) and Schmitz (1995). About 10 Sv are recirculated within the Atlantic whereas almost 15 Sv are entering the Southern Ocean south of 47.5°S. This water is then redistributed to the Indian and Pacific basins, where broad upwelling occurs. The model's overturning in the Southern Ocean is 25 Sv and within data-based estimates of 21 ± 6 Sv (Ganachaud and Wunsch, 2000). Temperature and salinity distributions are in good agreement with modern climatology (Levitus, 1982; Levitus et al., 1994; Levitus and Boyer, 1994), as are the distributions of DIC, ALK, PO_4 and other carbon-related oceanic tracers (Marchal et al., 1998a). Modeled specific inventories of anthropogenic carbon in the Atlantic Ocean for the years 1982 (North Atlantic) and 1989 (South Atlantic) are compared to data-based estimates (Gruber, 1998) (Fig. 1). The large overprediction of specific inventories at high latitudes can mainly be attributed to the simplified topography of the model, whereas the too small specific inventories in the low latitudes are due to a too weak thermocline ventilation (Gruber et al., 1996).

2.3. SRES emission scenarios and WRE stabilization profiles

We prescribe future emissions of CO_2, non-CO_2 GHGs and aerosols from the IPCC SRES emis-

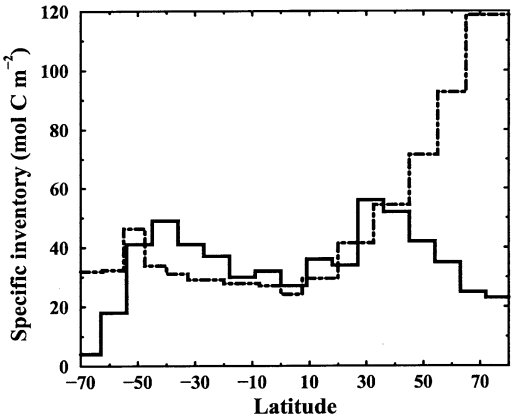

Fig. 1. Specific inventory of anthropogenic CO_2 in the Atlantic Ocean according to the data-based estimates of Gruber (1998) (solid) and the model estimates from the standard model simulation ($\Delta T_{2x} = 3.7°C$) (dot-dashed). North of the equator inventories are given for 1982; south of the equator they are given for 1989.

sion scenarios (Nakićenović et al., 2000). The SRES includes 40 emission scenarios for radiatively important gases until year 2100. These scenarios fall into four scenario "families". Each scenario "family" includes several quantifications of a common narrative. None of the SRES emission scenarios includes any future policies that explicitly address climate change. Here, we use the "Preliminary Marker Scenarios" A1, A2, B1, and B2 taken to be illustrative for each family, plus the scenarios with the highest (A1C-AIM) and lowest (B1T-MES) cumulative anthropogenic carbon emissions. The full range of the SRES scenarios is then covered in our model simulations.

The concentrations of CO_2 and non-CO_2 GHGs prescribed in the emission scenario simulations are based on observations up to year 1990. Then they are calculated from SRES emissions until 2100. Net land-use emissions are deduced from the atmospheric CO_2 budget until 1990 and then linearly interpolated to the SRES value at year 2000. The radiative forcing from changes in the concentration of well-mixed GHGs (CO_2, CH_4, N_2O, stratospheric H_2O and tropospheric O_3 owing to CH_4 changes, SF_6, 28 halocarbons including those controlled by the Montreal Protocol) and from direct and indirect effects of sulfate aerosols, is calculated based on simplified expressions (Harvey et al., 1997; Myhre et al., 1998; Fuglestvedt and Bernsten, 1999). The radiative forcing of black and organic carbon aerosols is assumed to be proportional to CO emissions, amounting to -0.06 W m^{-2} in year 1990.

We also present simulations where atmospheric CO_2 is prescribed according to the stabilization pathways WRE550 and WRE1000 (Wigley et al., 1997), where atmospheric CO_2 is stabilized at 550 and 1000 ppm, respectively. Prescribing atmospheric CO_2 allows us to quantify the strength of various global warming–marine carbon cycle feedback mechanisms associated with ocean carbon uptake.

3. Generic description of global warming–marine carbon cycle feedback mechanisms associated with ocean carbon uptake

The main driving force for the oceanic uptake of anthropogenic CO_2 is the increase in atmospheric pCO_2. However, the uptake of anthropogenic carbon and its distribution in the ocean are also influenced by changes in ocean circulation, sea-surface temperatures and salinities, and by changes in the marine biological cycle. The following physical and biogeochemical feedback mechanisms contribute to the differences in ocean CO_2 uptake between constant-climate simulations and global warming simulations in our model.

(1) "*SST feedback*": an increase in SST decreases the solubility of CO_2 in seawater, thereby reducing the oceanic uptake of CO_2. A warming of 1°C increases pCO_2 by about 4% at constant salinity, DIC, and ALK (Takahashi et al., 1993).

(2) "*Dilution feedback*": changes in air–sea freshwater fluxes dilute (or concentrate) surface concentrations of DIC, ALK, and nutrients. The changes in the water balance affect salinity, DIC concentrations, and ALK in the same proportions (Takahashi et al., 1980). The combined effects on pCO_2 of DIC and ALK changes nearly cancel each other. Dilution of surface salinity by 1 psu leads to a decrease in pCO_2 in the range of about 4 to 4.5% (Takahashi et al., 1993). However, on a global scale the "dilution feedback" is negligible as the global freshwater budget is balanced in the model.

(3) "*Circulation feedback*": a general slow-down in ocean circulation in the global warming simula-

tions reduces the surface-to-deep transport rate of excess carbon.

(4) "*Marine biota feedback*": changes in the cycling of marine OM and $CaCO_3$ alter surface DIC and ALK. An increase in DIC by 1% increases pCO_2 by about 10% (Revelle and Suess, 1957), whereas a 1% increase in ALK reduces pCO_2 by a similar amount (Takahashi et al., 1993). Biological production and the subsequent export of OM and $CaCO_3$ remove nutrients, DIC and ALK from the surface, remineralization adds these tracers again to the water column at depth; transport of remineralized material to the surface closes the two cycles. We differentiate the "marine biota feedback" into a "biota-OM feedback" associated with changes in the cycling of OM, and a "biota-$CaCO_3$ feedback" associated with changes in the cycling of $CaCO_3$.

(4a) "*Biota-OM feedback*": OM formation removes carbon from the DIC pool and adds ALK to the water by removing NO_3^-. Fluxes of PO_4, NO_3^-, ALK, and carbon in OM are related by constant Redfield ratios. The "biota-OM feedback" is the combination of two mechanisms. A decrease in surface PO_4 is associated with a decrease in surface DIC and pCO_2 that leads to a transient increase in ocean carbon uptake. We term this effect "biota-OM/DIC feedback". A decrease in surface PO_4 is also associated with an increase in surface ALK and a decrease in pCO_2 that tends to increase ocean carbon uptake. We term this much less important effect "biota-OM/ALK feedback". Changes in the OM cycle can be diagnosed by analyzing salinity-normalized PO_4 ($sPO_4 = PO_4 \cdot 34.73/S$) as the distribution of sPO_4 is not affected by gas exchange and freshwater fluxes and is only driven by the OM cycle in the model. In our terminology, the "biota-OM feedback" with respect to the uptake of CO_2 by the ocean is zero, if the surface field of sPO_4 remains unchanged during the simulation.

(4b) "*Biota-$CaCO_3$ feedback*": $CaCO_3$ removes ALK from the water by removing CO_3^{2-} and removes carbon from the DIC pool. A reduction in ALK due to a changed $CaCO_3$ cycle tends to decrease ocean carbon uptake that is only partially compensated by the associated reduction in surface DIC. We term the two effects "biota-$CaCO_3$/ALK feedback" and "biota-$CaCO_3$/DIC feedback", respectively. Changes in the $CaCO_3$ cycle can be diagnosed by analyzing salinity normalized alkalinities, sALK, corrected for ALK changes related to the OM cycle. The OM sALK corresponds to $16 \cdot sPO_4$, where 16 is the Redfield ratio between PO_4 and ALK of OM in our model. In this terminology, the biota-$CaCO_3$ feedback with respect to the uptake of CO_2 by the ocean is zero, if the surface field of $sALK + 16 \cdot sPO_4$ remains unchanged during the simulation.

Alternatively, we distinguish feedbacks with respect to changes in surface DIC and ALK instead of changes in the cycles of OM or $CaCO_3$.

(4a′) The "*biota-DIC feedback*' is the sum of the "biota-OM/DIC feedback" plus the much smaller "biota-$CaCO_3$/DIC feedback'.

(4b′) The "*biota-ALK feedback*' is the sum of the "biota-$CaCO_3$/ALK feedback" plus the much smaller "biota-OM/ALK feedback".

The different model configurations used to quantify the oceanic uptake of atmospheric CO_2 and the strength of the associated global warming–marine carbon cycle feedback mechanisms are described in detail in Table 2.

4. Results

4.1. SRES emission scenarios (1765–2100)

First, we project the evolution of ocean carbon uptake, atmospheric CO_2, radiative forcing, NADW formation and global-mean surface air temperature from preindustrial times up to year 2100 for the SRES emission scenarios (Fig. 2). The evolution of anthropogenic carbon emissions is identical for all SRES scenarios until present (Fig. 2a). In year 2100, global carbon emissions for the SRES scenarios range between 2.7 GtC yr^{-1} for the "technology driven" B1T-MES scenario and 36.6 GtC yr^{-1} for the "carbon intensive" A1C-AIM scenario. Cumulative anthropogenic carbon emissions for the 1990–2100 period vary between 764 GtC (B1T-MES) and 2511 GtC (A1C-AIM). In year 2100, half (49%) of the cumulated carbon emissions since the beginning of the industrial period is found in the atmosphere in the "Preliminary Marker Scenario" A1. The remainder is taken up by the ocean (32%) and the terrestrial biosphere (19%). Cumulative ocean carbon uptake from year 1765 until year 2100 ranges from 431 GtC (B1T-MES) to 716 GtC (A1C-AIM) for the SRES global warming simulations (Fig. 2b). The ongoing CO_2 emissions to the

Table 2. *Description of model configurations used to quantify the oceanic uptake of atmospheric CO_2 and the strength of the associated global warming–marine carbon cycle feedback mechanisms*

Simulation	Description of model setup
A	**Baseline; "no feedbacks"**: The climate sensitivity, ΔT_{2x}, is set to 0°C
B	**Standard; "all feedbacks"**: ΔT_{2x} is set to 3.7°C. SST, freshwater fluxes, ocean circulation, and biological cycling are described by prognostic formulations
C	**"SST feedback"**: The SST used to determine surface-water pCO_2 are from simulation B; all other parameters are as in the baseline simulation (simulation A)
D	**"SST" + "dilution feedback"**: As simulation C, but sea-surface salinities from simulation B are used to dilute/concentrate surface concentrations of DIC, ALK, total borate, etc. as in standard simulation B
E	**"SST" + "dilution" + "circulation feedback" = "no biota feedback"**: The physical model is used as in simulation B. The biological model is kept in a diagnostic mode where salinity normalized sea-surface PO_4, sPO_4, and salinity normalized sea-surface ALK, sALK, are restored towards steady state distributions. Then, the sPO_4 and sALK surface distributions are approximately the same as in simulation A and the "marine biota feedback" is excluded. A simulation with $\Delta T_{2x} = 3.7$°C, i.e., simulation E, and a control simulation where $\Delta T_{2x} = 0$°C are made. The results shown here are corrected for the slight difference between this control run and the baseline simulation A
F	**"SST" + "dilution" + "circulation" + "biota-$CaCO_3$/DIC feedback"**: As simulation E, but without restoring surface sALK towards preindustrial values. Surface sALK from the end of the regular model spin-up is used to determine surface-water pCO_2 in the chemistry routines. Changes in the carbon transport due to changes in $CaCO_3$ cycling are taken into account. A simulation with $\Delta T_{2x} = 3.7$°C, i.e., simulation F, and a control simulation where $\Delta T_{2x} = 0$°C are made. The results shown here are corrected for the slight difference between this control run and the baseline simulation A
G	**Constant ALK; "SST" + "dilution" + "circulation" + "biota-DIC feedback"**: Sea-surface pCO_2 is calculated using steady state values of sALK in the chemistry routines. All other parameters are as in the standard simulation B
H	**"No biota-OM/ALK feedback"**: ALK transported by OM is neglected. The model was spun up for 20,000 years, but without including OM ALK (the Redfield ratio of PO_4 to ALK of OM is set to 0). A simulation (simulation H) with all the other feedbacks included ($\Delta T_{2x} = 3.7$°C) and a control simulation similar to simulation A ($\Delta T_{2x} = 0$°C) are performed. Again, the results shown here are corrected for the slight difference between this control run and the baseline simulation A
I	**"Constant export"**: Export fluxes of OM and $CaCO_3$ are kept at their preindustrial values except when surface sPO_4 concentrations approach zero; then OM export is set to zero to avoid negative PO_4 concentrations
J	**Inorganic baseline; "no feedbacks"**: An inorganic model version that does not include formulations of the marine biosphere is applied. ΔT_{2x} is set to 0°C. Surface sALK is prescribed using the values of the baseline simulation A
K	**Inorganic standard; "SST" + "dilution" + "circulation feedback"**: As simulation J, but with $\Delta T_{2x} =$ 3.7°C
L	**"Circulation" + "dilution feedback"**: SST used to calculate surface pCO_2 are kept at preindustrial values while all other parameters are as in simulation E. Then, both the "SST" and the "marine biota feedback" are excluded and only the 'circulation' and 'dilution feedback' are operating in the model. A simulation with $\Delta T_{2x} = 3.7$°C, i.e., simulation L, and a control simulation where $\Delta T_{2x} =$ 0°C are made. The results shown here are slightly corrected as explained for simulation E
M	**'Circulation" + "SST feedback"**: Salinities used to calculate the surface pCO_2 are kept at preindustrial values while all other parameters are as in simulation E. Then, both the "dilution" and the "marine biota feedback" are excluded and only the "circulation" and the "SST feedback" are operating in the model. A simulation with $\Delta T_{2x} = 3.7$°C, i.e., simulation M, and a control simulation where $\Delta T_{2x} = 0$°C are made. The results shown here are slightly corrected as explained for simulation E
N	**"Circulation feedback"**: SST as well as surface salinities used to calculate surface pCO_2 are kept at preindustrial values while all other parameters are as in simulation E. Then, the "SST", "dilution" and "marine biota feedback" are excluded and only the "circulation feedback" is operating in the model. A simulation with $\Delta T_{2x} = 3.7$°C, i.e., simulation N, and a control simulation where $\Delta T_{2x} =$ 0°C are made. The results shown here are slightly corrected as explained for simulation E

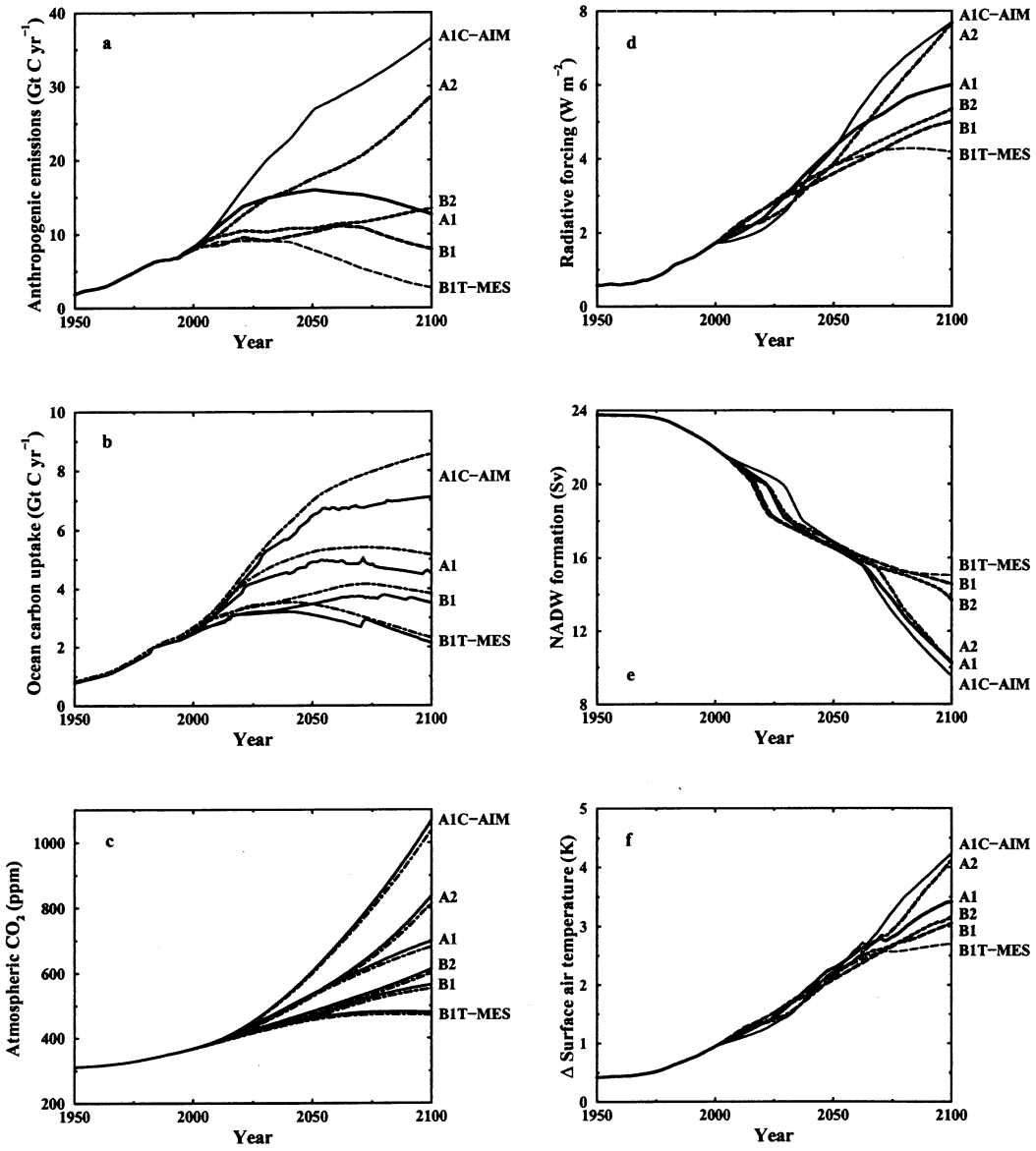

Fig. 2. (a) Prescribed anthropogenic carbon emissions and (b) projected ocean carbon uptake, (c) atmospheric CO_2, (d) radiative forcing by CO_2 and non-CO_2 agents, (e) formation of North Atlantic Deep Water (NADW), and (f) increase in global-mean air temperature for the standard model setup ($\Delta T_{2x} = 3.7°C$). The different curves correspond to the IPCC SRES "Preliminary Marker Scenarios" A1, A2, B1, B2 and the scenarios A1C-AIM and B1T-MES. Projected ocean carbon uptake and atmospheric CO_2 from the constant-climate baseline simulations ($\Delta T_{2x} = 0°C$) are shown by dot-dashed lines in (b) and (c). Results for the scenarios A2 and B2 are not shown in (b) for clarity.

atmosphere result in a projected increase in atmospheric CO_2 concentrations from 351 ppm in year 1990 to 471 ppm at the end of the 21st century for B1T-MES and to 1071 ppm for A1C-AIM (Fig. 2c). The radiative forcing by CO_2, non-CO_2 GHGs and aerosols increases by 4 W m^{-2} (B1T-MES) to 8 W m^{-2} (A1C-AIM) from 1990 to 2100 (Fig. 2d). This leads to an increase in global-mean surface air temperature between 2.7°C (B1T-MES) to 4.3°C (A1C-AIM; Fig. 2f) and to a decrease in NADW formation by 40% (B1T-MES) to 62% (A1C-AIM; Fig. 2e). Paradoxically, radiative forcing is lowest during the next three decades for the scenario with the highest carbon emissions (A1C-AIM). This is because of a strong negative forcing caused by high sulfur emissions. Atmospheric CO_2 and radiative forcing due to GHGs and aerosols continue to increase in year 2100 in all SRES scenarios, except in B1T-MES, the scenario with the lowest carbon emissions.

The CO_2 uptake by the ocean is reduced in simulations with global warming compared to simulations assuming constant climate. Oceanic carbon uptake for 1980–1989 and 1990–1999 is 2.00 GtC yr^{-1} and 2.32 GtC yr^{-1}, respectively, for the SRES global warming simulations with $\Delta T_{2x} = 3.7$°C. It is 2.08 GtC yr^{-1} and 2.45 GtC yr^{-1}, respectively, for the constant-climate simulations with $\Delta T_{2x} = 0$°C. In year 2100, the ocean uptake is reduced by 0.1 GtC yr^{-1} (B1T-MES) to 1.5 GtC yr^{-1} (A1C-AIM) due to global warming (Fig. 2b). The projected reduction in cumulative CO_2 uptake due to global warming until year 2100 is between 7% (B1T-MES) and 10% (A1C-AIM) for the SRES emission scenarios. The resulting difference in projected atmospheric CO_2 is around 4% (Fig. 2c) consistent with results found earlier for the IS92 emission scenarios (Joos et al., 1999). Here, we explicitly consider the contribution of non-CO_2 agents to radiative forcing that were assumed to be zero for the IS92 scenarios (Wigley et al., 1997). We note that the reduction in projected atmospheric CO_2 is small compared to results from studies that address global warming-terrestrial carbon cycle feedbacks (Cox et al., 2000; Lenton, 2000; Friedlingstein et al., 2001).

4.2. *WRE stabilization profiles (1765–2500)*

The CO_2 stabilization profiles WRE550 and WRE1000 are applied (Fig. 3a). The evolution of atmospheric CO_2 up to year 2100 in WRE550 and WRE1000 is, at least to some extent, comparable to that simulated for the "Preliminary Marker Scenarios" B1 and A1. Atmospheric CO_2 concentrations at the end of the 21st century are 540 ppm for WRE550 (565 ppm in scenario B1) and 673 ppm for WRE1000 (699 ppm in scenario A1). However, projected global-mean air temperatures in the WRE simulations at year 2100 are almost 0.7°C lower than in the scenarios A1 and B1, predominantly because the radiative forcing of non-CO_2 agents is not considered in the WRE simulations. Accordingly, circulation changes until year 2100 are smaller in the WRE cases compared to the SRES cases (Figs. 2e and 3b). Nevertheless, significant circulation changes occur in both WRE550 and WRE1000 relative to the steady state (Figs. 4a, b). The NADW formation in both WRE cases is reduced by about 40% until year 2100 (Fig. 3b).

Simulations are extended to year 2500 to investigate potential long-term changes in ocean circulation and ocean carbon cycle. The strength of NADW formation is further reduced after year 2100 in the WRE1000 global warming simulation (Fig. 3b). In WRE550, NADW formation partially recovers until year 2500, whereas in WRE1000 it is almost completely shut off at year 2300 and does not recover during another 5000 years of integration. The permanent collapse of the THC in simulation WRE1000 indicates that the ocean circulation settled into a structurally different equilibrium state (Fig. 4c). The modeled changes in ocean circulation as well as in ocean temperature and salinity in simulation WRE1000 until year 2500 are qualitatively similar to those of Schmittner and Stocker (1999) using the same climate model.

The various global warming feedbacks reduce the oceanic uptake of CO_2 by nearly 8% by year 2100 in both stabilization simulations (simulation A–B; Table 3 and Figs. 3c,d), similar to the SRES scenarios. By year 2500, the reduction increases to 16% (WRE550) and 24% (WRE1000). The deduced anthropogenic carbon emissions by year 2100 are reduced by 41 GtC for WRE550 and by 48 GtC for WRE1000 in global warming simulations compared to constant-climate baseline simulations. This corresponds to a reduction of about 3% for both WRE cases due to global warming. By year 2500, the deduced

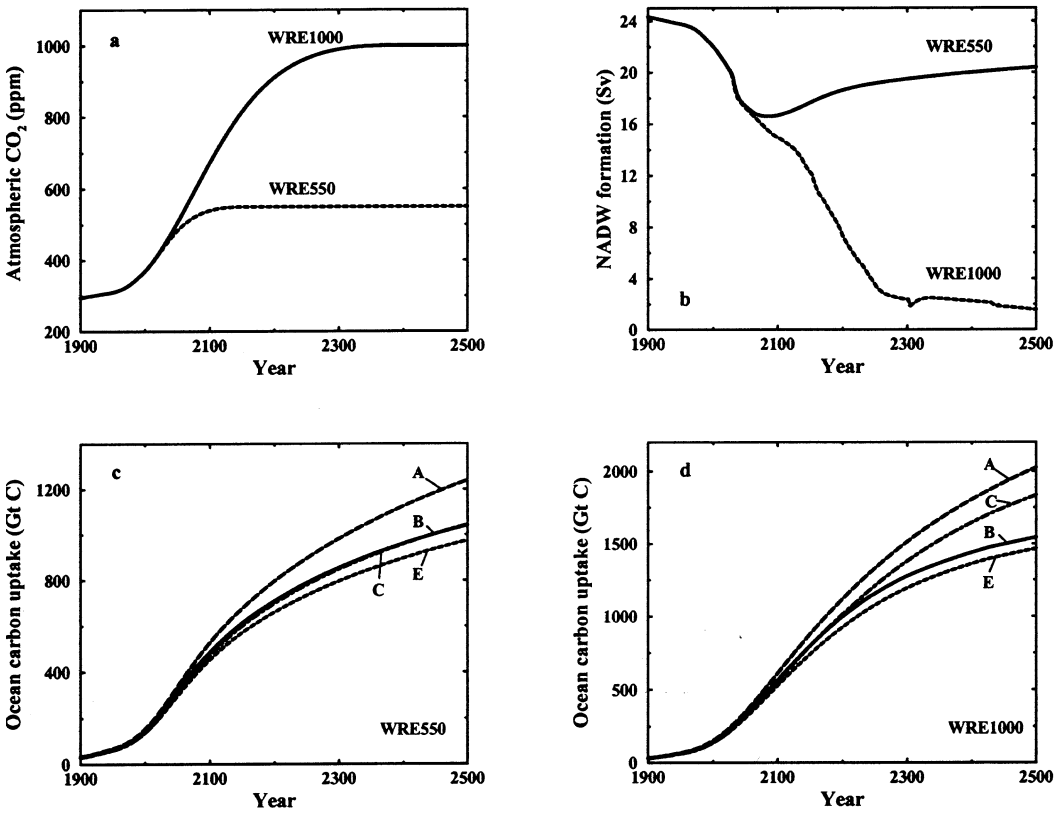

Fig. 3. (a) Prescribed atmospheric CO_2, (b) projected formation of North Atlantic Deep Water (NADW), and projected cumulative ocean carbon uptake for stabilization profiles WRE550 (c) and WRE1000 (d) and the standard model setup ($\Delta T_{2x} = 3.7°C$). The projected cumulative ocean carbon uptake for the constant-climate baseline simulation ($\Delta T_{2x} = 0°C$) is shown by long-dashed lines. The simulations C (dot-dashed) and E (dashed) are used to identify different global warming feedback mechanisms (Tables 2, 3). Results for simulation D are not shown in (c) and (d) for clarity.

emissions are reduced by 198 GtC for WRE550 and 392 GtC for WRE1000, corresponding to a 9% reduction for both WRE profiles.

4.3. *Changes in ocean circulation and tracer distributions*

In this Subsection, we analyze ocean circulation changes and changes in the oceanic tracer distributions in more detail for the stabilization profile WRE1000.

4.3.1. *Changes in physical properties*

4.3.1.1. Circulation. The changes in ocean circulation at year 2100 compared to the preindustrial steady state are largest in the North Atlantic, where the overturning cell is shallower and substantially reduced in strength (Figs. 4a, b). By year 2100 the deep Atlantic Ocean below 2000 m is dominated by a counterclockwise circulation cell, indicating increasing influence of Southern Ocean water. Circulation changes in the Pacific and Indian oceans as well as in the Southern Ocean are comparatively modest. Circulation changes in the Pacific and Indian basins are most pronounced around 40°S between 1000 and 3000 m depth.

4.3.1.2. Temperature and salinity. By year 2100, significant temperature and salinity anomalies have developed (Figs. 5a, b). The time scale of the anthropogenic atmospheric forcing is generally faster than the time scale on which the ocean

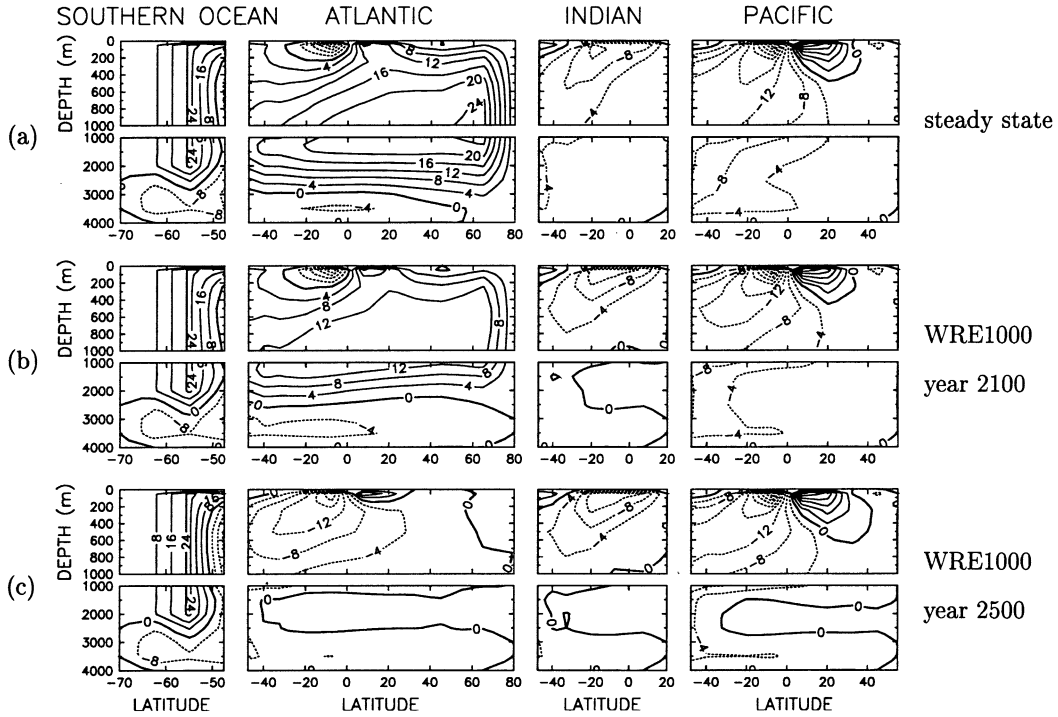

Fig. 4. Meridional overturning streamfunction (Sv) in the Southern Ocean and in the Atlantic, Indian and Pacific basins at different times. (a) Preindustrial steady state (year 1765), (b) year 2100 and (c) year 2500 for CO_2 stabilization profile WRE1000. Results in (b) and (c) are produced with the standard model setup ($\Delta T_{2x} = 3.7°C$). Contour interval is 8 Sv in the Southern Ocean and 4 Sv in the Atlantic, Indian and Pacific basins.

mixes the additional heat and freshwater to the deep ocean, except in regions where convection occurs (Schmittner and Stocker, 1999). In year 2100, the excess heat has penetrated the upper 1000 m of the ocean (Fig. 5a). The modeled increase of SST ranges between 1.2 and 3.1°C, with maximum warming in the North Pacific, the equatorial regions and in the Southern Ocean (Fig. 6a). The sea-surface warming is much smaller in the northern North Atlantic compared to the rest of the surface ocean. The SST increase of 1.2°C north of 65°N is by at least 0.6°C smaller than the SST increase elsewhere. This significant damping of the SST perturbation is predominantly due to convective mixing of excess heat to depth and the reduction in poleward heat transport associated with the slow-down in Atlantic meridional overturning. The maximum temperature increase in year 2100 (about +3.3°C) is found in the North Atlantic subsurface waters at 400 m between 40° and 65°N and in the North Pacific top 100 m north of 35°N. Salinity increases predominantly at low latitudes, whereas the high-latitude surface waters get fresher in both hemispheres as a consequence of an enhanced hydrological cycle in the warmer atmosphere (Fig. 5b). The modeled surface salinity changes until year 2100 range between −0.5 psu (North Pacific) and +0.8 psu (subtropical regions of the Indian). The North Atlantic surface waters north of 40°N have freshened by 0.4 psu at that time.

4.3.2. Changes in biogeochemical properties

4.3.2.1. Phosphate. First, we analyze changes in sPO_4 until year 2100 for stabilization profile WRE1000 (Fig. 5c). Recall that sPO_4 is only affected by changes in the cycling of OM and that the ratio of P to C is taken to be constant in OM. In general, sPO_4 concentrations are decreased in the upper ocean and increased in the deep ocean relative to preindustrial times. In the deep North Atlantic sPO_4 is increased by more than

Table 3. *Ocean carbon uptake for different model configurations and the WRE1000 CO_2 stabilization profile, and reduction in CO_2 uptake due to the main global warming-marine carbon cycle feedback mechanisms*

Simulation	Model setup	1980–1989	1765–2100	1765–2500
Model experiments: cumulative ocean uptake (Gt of C)				
A	baseline (no feedbacks; $\Delta T_{2x} = 0°C$)	21.4	612	2027
B	standard (all feedbacks; $\Delta T_{2x} = 3.7°C$)	20.2	564	1545
C	SST	19.4	554	1837
D	SST + dilution	19.4	555	1891
E	SST + dilution + circulation	19.2	528	1467
F	SST + dilution + circulation + biota-$CaCO_3$/DIC	19.3	532	1522
G	SST + dilution + circulation + biota-DIC	20.5	577	1696
H	SST + dilution + circulation + biota-DIC + biota-$CaCO_3$/ALK	20.1	559	1531
I	constant export fluxes	20.5	581	1609
J	inorganic model, baseline	22.4	648	2202
K	inorganic model, standard	20.1	556	1652
L	dilution + circulation	21.2	584	1735
M	SST + circulation	19.2	527	1469
N	circulation	21.2	584	1737
Estimated reduction in ocean uptake by main feedbacks (%)				
A–C	SST	9.4	9.5	9.4
C–D	dilution	0.0	−0.2	−2.7
D–E	circulation	0.9	4.5	20.9
E–B	biota	−4.7	−5.9	−3.8
A–B	total reduction	5.6	7.9	23.8
Independent estimates for reduction in ocean uptake by feedbacks (%)				
A–C	SST	9.4	9.5	9.4
L–E	SST	9.4	9.2	13.3
C–D	dilution	0.0	−0.2	−2.7
M–E	dilution	0.0	−0.1	0.1
D–E	circulation	0.9	4.5	20.9
A–N	circulation	0.9	4.7	14.3
A–E	SST + dilution + circulation	10.3	13.8	27.6
J–K	SST + dilution + circulation	10.3	14.2	25.0

A description of the different model configurations is given in Table 2. The reduction in ocean uptake due to different feedback mechanisms is estimated as difference between corresponding simulations as a percentage of the uptake obtained by running the baseline simulations A or J. See Section 3 for an explanation of the feedback mechanisms associated with the uptake of atmospheric CO_2 by the ocean. The attribution of the reduction in oceanic CO_2 uptake to different mechanisms is only an approximation as the ocean–atmosphere carbon cycle system is non-linear. The validity of this approximation is checked by comparing independent estimates of the feedback strength as obtained by Sim. A to H, by the inorganic model (Sim. J and K) and by, e.g., simulations L to N.

0.6 mmol m^{-3}. The positive deep North Atlantic anomalies result primarily from the decrease in the ventilation by PO_4-poor NADW and a stronger influence of PO_4-rich waters of Antarctic origin (Marchal et al., 1998b; Marchal et al., 1999b). Euphotic zone sPO_4 is reduced by up to 0.1 mmol m^{-3}, with larger reductions occurring at latitudes where large changes in ocean circulation are modeled, such as in the Pacific and Indian basins around 40°S and in the North Atlantic north of 50°N (Fig. 6b). The North Atlantic reduction in euphotic zone sPO_4 largely increases with increasing latitude, ranging from below 0.1 mmol m^{-3} at 40°N to 0.5 mmol m^{-3} at 80°N. This general reduction in euphotic zone sPO_4 is attributable to the slowed ocean circulation. Nutrient supply to the surface is reduced owing to the decrease in vertical transport and the residence time of water in the euphotic zone is increased, allowing for a larger fraction of the

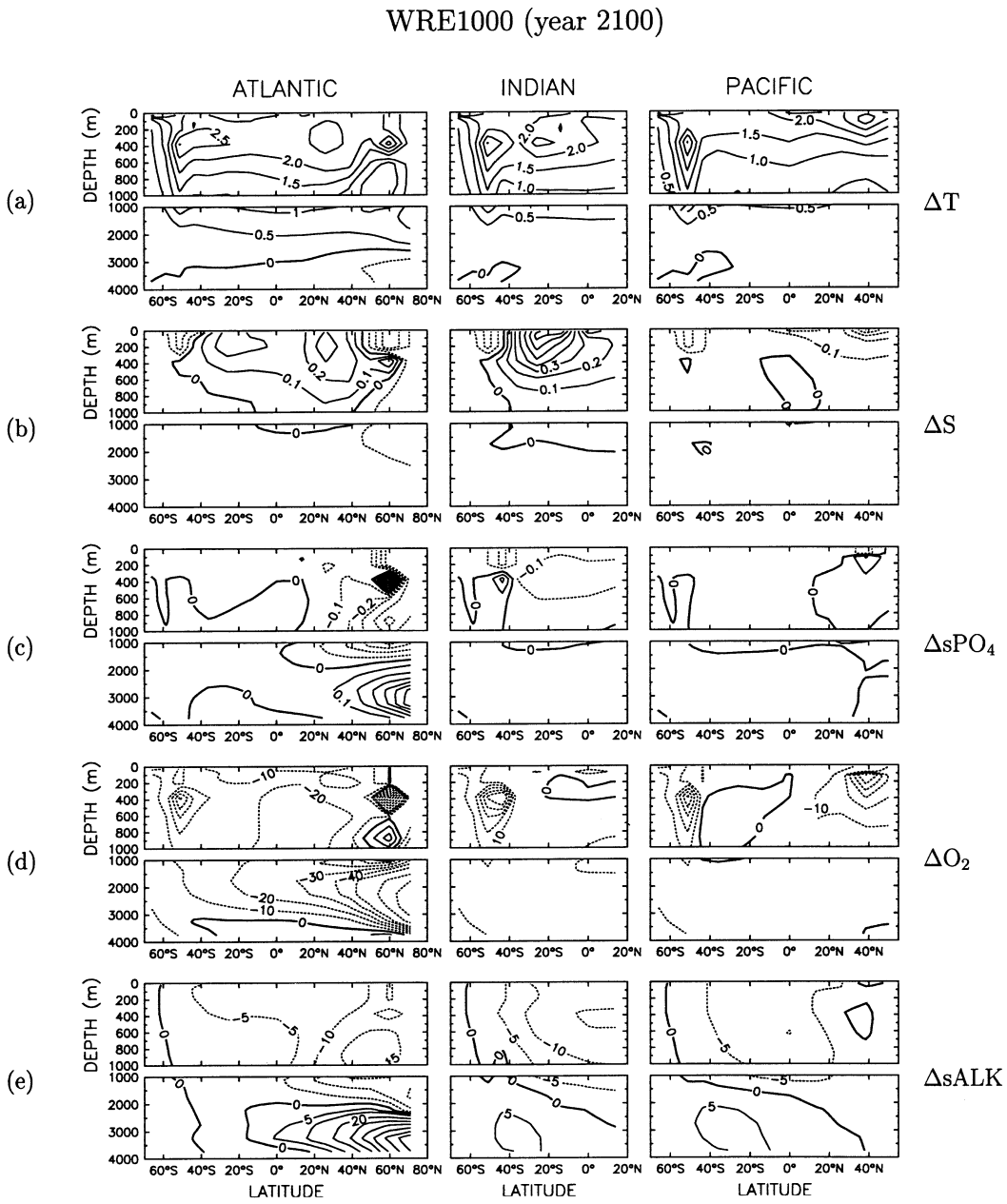

Fig. 5. Latitude-depth distribution of changes in physical and biogeochemical properties in the three main oceanic basins at year 2100 relative to the preindustrial steaty state. (a) Ocean temperature (K), (b) ocean salinity (psu), (c) salinity-normalized PO_4 (sPO_4 in mmol m^{-3}), (d) O_2 (mmol m^{-3}) and (e) salinity-normalized ALK (sALK in meq m^{-3}). Results are shown for the standard model setup ($\Delta T_{2x} = 3.7°C$) and CO_2 stabilization scenario WRE1000. Contour intervals in (d) and (e) are unequally spaced for clarity. Contour intervals and applied ranges are as follows: (a) 0.5°C from −1 to +3.5, (b) 0.1 psu from −0.5 to +0.8, (c) 0.1 mmol m^{-3} from −0.6 to +0.7, (d) 20 mmol m^{-3} from −170 to −50 and 10 mmol m^{-3} from −50 to +30, and (e) 5 meq m^{-3} from −30 to +10 and 10 meq m^{-3} from +10 to +80.

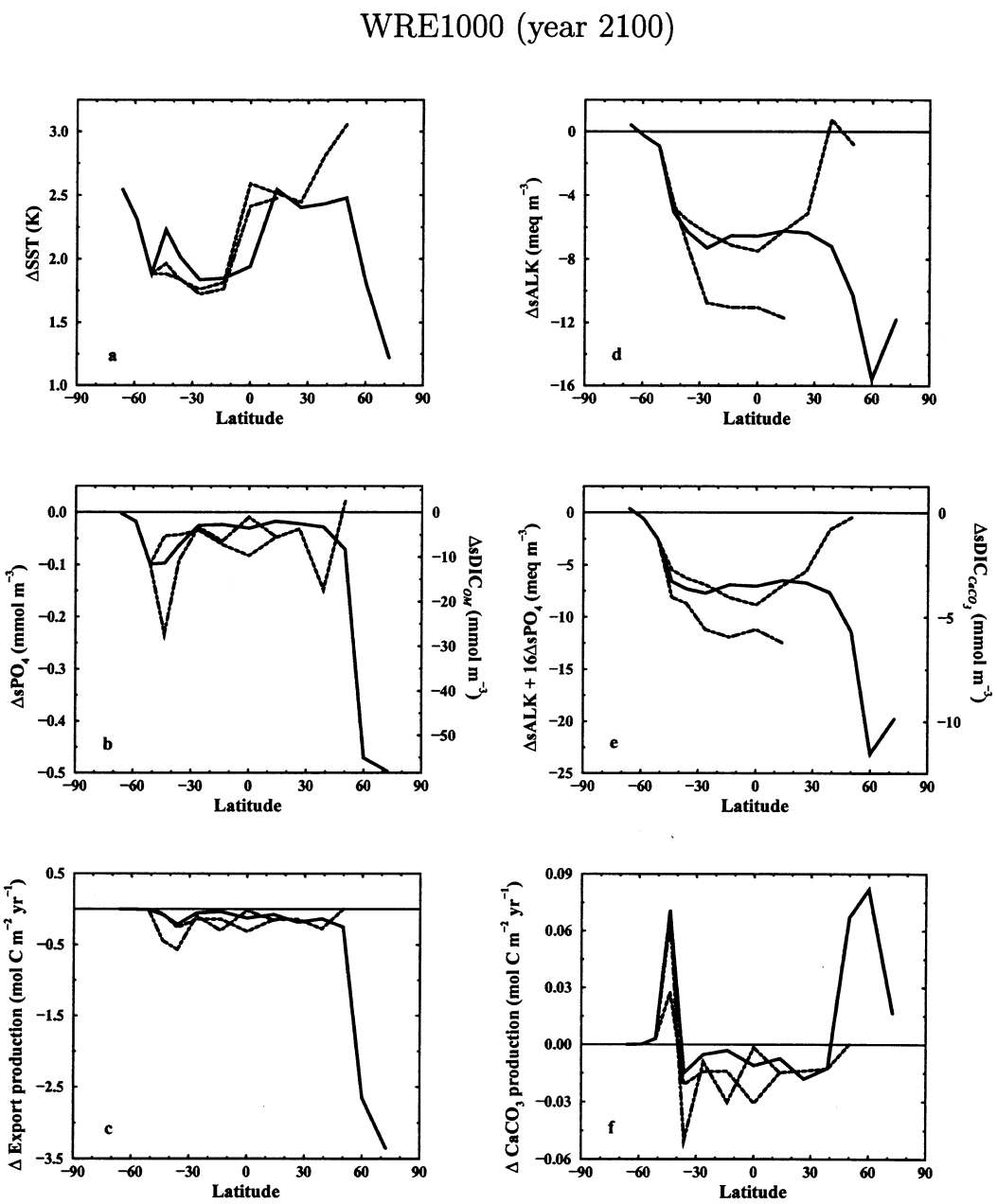

Fig. 6. Latitudinal distribution of changes in (a) sea-surface temperatures, (b) salinity-normalized euphotic zone PO_4, sPO_4, (c) export production of organic matter (OM), (d) salinity-normalized euphotic zone ALK, sALK, (e) salinity-normalized euphotic zone ALK from changes in the $CaCO_3$ cycle, and (f) $CaCO_3$ production in the three main oceanic basins until year 2100. Results are shown for the standard model setup ($\Delta T_{2x} = 3.7°C$) and stabilization scenario WRE1000. The different curves classify the Atlantic (solid), Indian (dot-dashed) and Pacific (dashed) basins. In panels (c) and (d) the right axis indicates the range of related changes in salinity-normalized DIC due to the internal reorganization of the OM cycle, $\Delta sDIC_{OM}$, and due to the internal reorganization of the $CaCO_3$ cycle, $\Delta sDIC_{CaCO_3}$.

supplied nutrients to be taken up biologically. Export production of OM is also reduced at all latitudes (Fig. 6c). The reduction in global export production for WRE1000 is nearly 0.9 GtC yr^{-1} by the end of the century, dropping from 13.1 GtC yr^{-1} in year 1765 to 12.2 GtC yr^{-1} in year 2100. sPO_4 is reduced in surface waters, despite reduced export fluxes.

4.3.2.2. Oxygen. Closely related to changes in the distribution of PO_4 are changes in the distribution of dissolved O_2 (Fig. 5d). Changes in OM cycling cause inverse changes in O_2 and PO_4 concentrations. Changes in the O_2 air–sea gas exchange further modify the oceanic O_2 distribution. In the Southern Ocean top 1000 m, O_2 is significantly reduced, whereas sPO_4 remains nearly unchanged. At year 2100, a maximum reduction in O_2 of 160 mmol m^{-3} is simulated in the North Atlantic between 400 and 600 m depth. In the deep North Atlantic the O_2 reduction reaches nearly 120 mmol m^{-3}. In Subsection 4.5 we will address the modeled changes in the oceanic oxygen inventory and discuss possible implications for the interpretation of atmospheric O_2/N_2 measurements.

4.3.2.3. Alkalinity. Next, we analyze changes in ALK at year 2100 for WRE1000 (Fig. 5e). Changes in sALK are largely determined by changes in the cycling of $CaCO_3$ and, to a lesser extent, by changes in the cycling of OM. In general, sALK (and $sALK + 16 \cdot sPO_4$) is reduced in the upper ocean and increased in the deep ocean. The euphotic zone sALK (and $sALK + 16 \cdot sPO_4$) is reduced at almost all latitudes (Figs. 6d,e). Again, we ascribe this general reduction to the longer residence time of waters in the euphotic zone and the associated more effective biological utilization of CO_3^{2-} through $CaCO_3$ production. The global export of $CaCO_3$ decreases until year 2100 by 0.03 GtC yr^{-1} from the preindustrial flux of 1.17 GtC yr^{-1}. The production largely increases at high latitudes (Fig. 6f) relative to the preindustrial steady state. This is related to a significant increase in the ratio of $CaCO_3$ to OM formation (production ratio), that is assumed to be temperature dependent in our model (Marchal et al., 1998a). However, we consider this model feature as highly uncertain. Similar to the large positive sPO_4 anomalies, sALK is increased significantly in the deep North Atlantic (by over 70 meq m^{-3}) following the decrease in the ventilation by NADW. Many other parts of the deep ocean below 2000 m show an increase in sALK by a few meq m^{-3}.

4.3.2.4. Dissolved inorganic carbon. The oceanic DIC inventory increases in response to rising atmospheric CO_2. Changes in DIC are largest at the ocean surface and decrease with depth in both the simulation with and without global warming (Figs. 7a,b). Significant DIC changes in the deep water of the North Atlantic and the Southern Ocean reflect the relatively fast surface-to-deep mixing in those areas, but also changes in the biological cycles in the global warming simulation.

The change in the oceanic distribution of salinity-normalized DIC, $\Delta sDIC$, of the global warming simulation is attributed to (1) the uptake of carbon from the atmosphere by air–sea gas exchange, $\Delta sDIC_{gas}$ (Figs. 7b,c), (2) the changes due to the internal reorganization of the OM cycle, $\Delta sDIC_{OM}$, (Fig. 7d), and (3) the changes due to the internal reorganization of the $CaCO_3$ cycle, $\Delta sDIC_{CaCO_3}$ (Fig. 7e) (Gruber and Sarmiento, 2001).

The change in sDIC caused by the internal reorganization of the OM cycle, $\Delta sDIC_{OM}$, is calculated by multiplying ΔsPO_4 (Fig. 5c) by the Redfield ratio C to P of 117:

$$\Delta sDIC_{OM} = 117 \cdot \Delta sPO_4. \quad (3)$$

The change in sDIC caused by the internal reorganization of the $CaCO_3$ cycle, $\Delta sDIC_{CaCO_3}$, is calculated by multiplying $\Delta sALK + 16 \cdot \Delta sPO_4$ (Figs. 5c,e) by 0.5 (ratio C to ALK of $CaCO_3$):

$$\Delta sDIC_{CaCO_3} = 0.5 \cdot (\Delta sALK + 16 \cdot \Delta sPO_4). \quad (4)$$

Thereby, the response in air–sea gas exchange to changes in the biological cycles is not taken into account in $\Delta sDIC_{OM}$ and $\Delta sDIC_{CaCO_3}$. The total ocean inventory of $\Delta sDIC_{OM}$ and $\Delta sDIC_{CaCO_3}$ is zero (cf. numbers to the right of Figs. 7d,e). Analogous to the changes in sPO_4 and sALK discussed above, sDIC is reduced in the upper ocean and increased in the deep ocean due to the internal reorganization of the biological cycles. The largest changes occur again in the North Atlantic and are associated with the reduction in the penetration of NADW to depth.

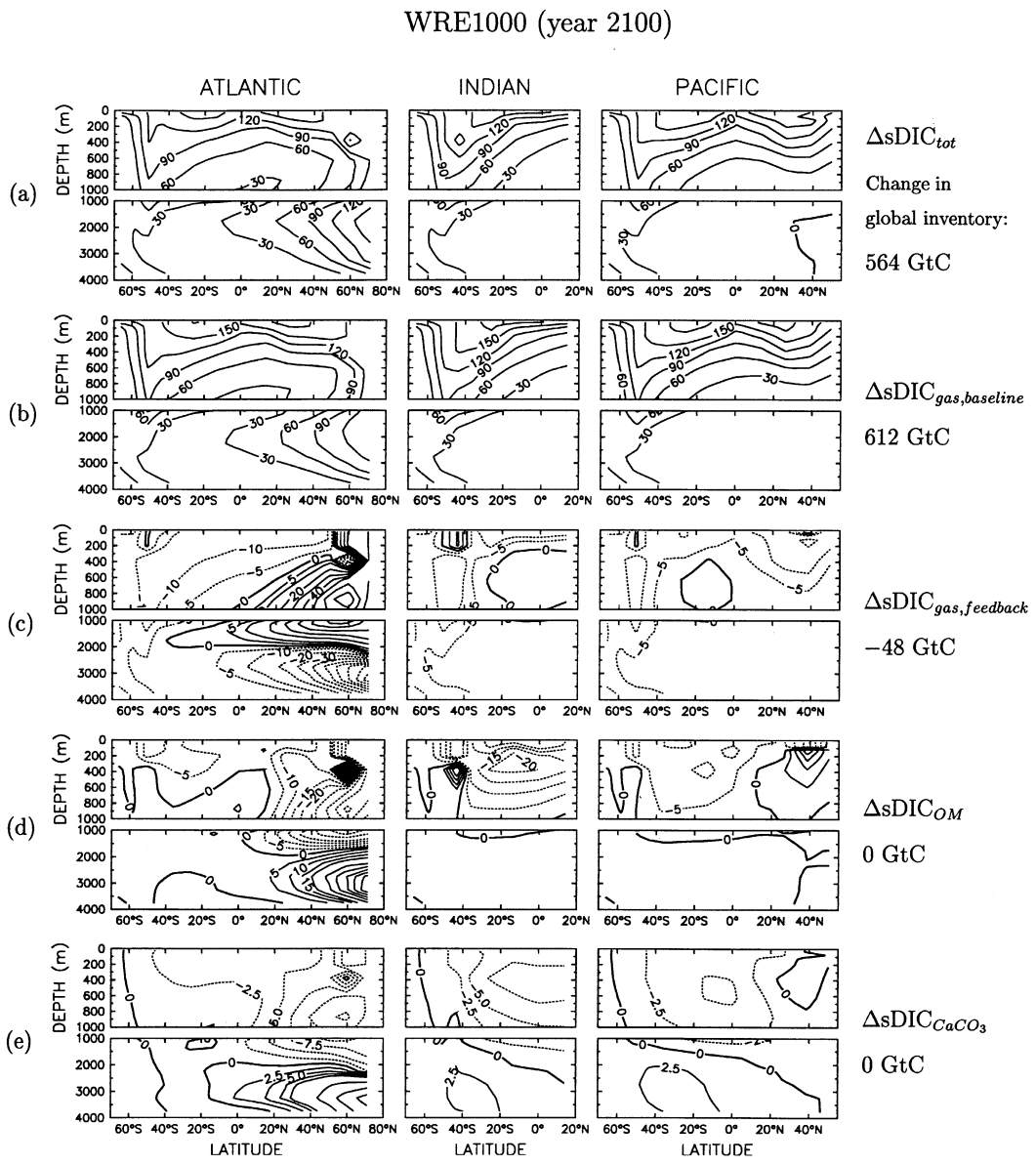

Fig. 7. Latitude-depth distribution of changes in salinity-normalized DIC (sDIC) in the three main oceanic basins until year 2100. (a) Total change in sDIC (ΔsDIC$_{tot}$ in mmol m^{-3}) from the standard model setup ($\Delta T_{2x} = 3.7°C$), (b) excess sDIC due to gas exchange only (ΔsDIC$_{gas,baseline}$ in mmol m^{-3}) from the constant-climate baseline simulation ($\Delta T_{2x} = 0°C$) compared to the preindustrial steady state, (c) ΔsDIC due to the changes in air–sea gas exchange (ΔsDIC$_{gas,feedback}$ in mmol m^{-3}), (d) ΔsDIC due to the internal reorganisation of the OM cycle (ΔsDIC$_{OM}$ in mmol m^{-3}), and (e) ΔsDIC due to the internal reorganisation of the $CaCO_3$ cycle (ΔsDIC$_{CaCO_3}$ in mmol m^{-3}) at year 2100 from the standard model setup ($\Delta T_{2x} = 3.7°C$) compared to the constant-climate baseline simulation ($\Delta T_{2x} = 0°C$). All the results given are for the CO_2 stabilization profile WRE1000. sDIC inventory changes (GtC) are indicated to the right of the panels. Contour intervals in (c), (d) and (e) are unequally spaced for clarity. Contour intervals and applied ranges are as follows: (a) and (b) 30 mmol m^{-3} from 0 to +190, (c) 10 mmol m^{-3} from −100 to −10, 5 mmol m^{-3} from −10 to +10 and 10 mmol m^{-3} from +10 to +80, (d) 10 mmol m^{-3} from −90 to −20, 5 mmol m^{-3} from −20 to +20 and 10 mmol m^{-3} from +20 to +90, and (e) 2.5 mmol m^{-3} from −20 to +10 and 10 mmol m^{-3} from +10 to +50.

The changes in sDIC related to CO_2 uptake from the atmosphere by gas exchange, $\Delta sDIC_{gas}$, are further attributed to the global warming feedbacks introduced in Section 3 ($\Delta sDIC_{gas,feedback}$; Fig. 7c) and to the gas exchange modeled assuming constant climate ($\Delta sDIC_{gas,baseline}$; Fig. 7b). $\Delta sDIC_{gas,feedback}$ is calculated by subtracting $\Delta sDIC_{gas,baseline}$, $\Delta sDIC_{OM}$ and $\Delta sDIC_{CaCO_3}$ from $\Delta sDIC$ of the global warming simulation ($\Delta sDIC_{tot}$; Fig. 7a):

$$\Delta sDIC_{gas,feedback} = \Delta sDIC_{tot} - \Delta sDIC_{gas,baseline} - \Delta sDIC_{OM} - \Delta sDIC_{CaCO_3}. \quad (5)$$

The total ocean inventory of $\Delta sDIC_{gas,feedback}$ is -48 GtC and corresponds to the total reduction in ocean uptake between the simulation with and without global warming (Table 3). This reduction is caused by the global warming feedbacks further discussed in the following Subsection 4.4 ("SST", "dilution", "circulation", and "marine biota feedback"). In most ocean regions the feedbacks act to reduce sDIC and $\Delta sDIC_{gas,feedback}$ is negative. In the Southern Ocean the $\Delta sDIC_{gas,feedback}$ signal penetrates down to the bottom. In the North Atlantic $\Delta sDIC_{gas,feedback}$ shows a dipole structure similar to that seen for ΔsPO_4 and $\Delta sALK$, but of opposite sign. The reduction in NADW prevents carbon that entered the ocean by gas exchange to be transported to the deep North Atlantic and more of this carbon remains above 2000 m. This yields large positive values of $\Delta sDIC_{gas,feedback}$ in the upper 2000 m of the North Atlantic with a maximum value of almost 80 mmol m^{-3} and large negative values below (nearly -100 mmol m^{-3} at minimum).

The $\Delta sDIC$ distribution in the North Atlantic is similar in simulations with global warming and in simulations without it (Figs. 7a,b), despite significant circulation changes. This can now be understood as the result of two opposing mechanisms. The reduction in the magnitude and the penetration depth of NADW leads to shallower penetration and to an accumulation in the upper ocean of carbon that enters the North Atlantic by air–sea gas exchange. Changes in NADW formation cause changes in the biological cycles that lead to a decrease in sDIC in the upper ocean and to an increase in sDIC in the deep ocean.

For simplicity, we only show salinity normalized DIC concentrations in Figs. 7a–e. The changes in DIC caused by changes in salinity can be inferred from Fig. 5b. A salinity change of 0.1 psu corresponds roughly to a DIC change of 7 mmol m^{-3}. The changes in DIC due to salinity changes are of similar magnitude as the changes in $\Delta sDIC_{OM}$ and $\Delta sDIC_{CaCO_3}$.

4.4. *Quantification of global warming–marine carbon cycle feedback mechanisms associated with ocean carbon uptake*

In Subsection 4.3, we have discussed the changes in the distribution of various tracers within the ocean due to global warming for the stabilization profile WRE1000 at year 2100. It has become clear, how the uptake of heat and large-scale changes in circulation, in the freshwater cycle, and in the cycles of OM and $CaCO_3$ affect surface-water composition and properties. These changes in SST, surface salinity, $\Delta sALK$, $\Delta sDIC_{OM}$, and $\Delta sDIC_{CaCO_3}$ (Fig. 6) affect surface pCO_2 and the uptake of CO_2 by the ocean, in addition to changes in surface-to-deep transport rates. In this section, we focus on the ocean–atmosphere interface and analyze how global warming affects net air–sea carbon fluxes for WRE550 and WRE1000. We investigate the strength of global warming feedback mechanisms associated with the oceanic CO_2 uptake by analyzing simulations with global warming and simulations without it. In particular, we quantify regionally the changes in oceanic CO_2 uptake for the combined global warming feedbacks as well as for the various individual global warming feedbacks introduced in Section 3.

4.4.1. Combined feedback mechanisms. As mentioned before the combined global warming–marine carbon cycle feedbacks reduce ocean carbon uptake in the stabilization simulations globally by 8% until year 2100 and by 16% (WRE550) and 24% (WRE1000) until year 2500. Here, we analyze the geographic structure of this reduction until year 2500 (Fig. 8). In general, tropical and subtropical regions between 32.5°S and 32.5°N, covering about 60% of the total ocean surface area, determine the reduction in CO_2 uptake in the 1765–2500 period in our model. However, changes per unit area occurring at high latitudes of the North Atlantic and in the Southern Ocean exceed changes in the tropics and subtrop-

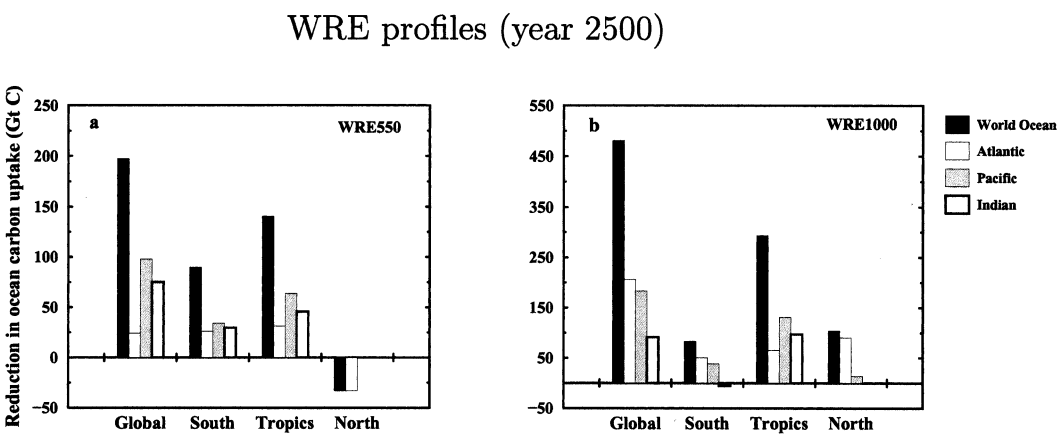

Fig. 8. Reduction in oceanic carbon uptake in the world ocean and the three main oceanic basins due to global warming until year 2500. The reduction is given for the standard model setup ($\Delta T_{2x} = 3.7°C$) and stabilization profiles WRE550 (a) and WRE1000 (b) compared to the constant-climate baseline ($\Delta T_{2x} = 0°C$). Contributions from individual ocean basins and the world ocean are shown for three latitudinal regions (South: 70°S–32.5°S; Tropics: 32.5°S–32.5°N; North: 32.5°N–80°N). Positive values stand for a reduction and negative values for an increase in ocean CO_2 uptake.

ics. The total reduction in ocean CO_2 uptake by year 2100 (not shown) is of similar magnitude in tropical and subtropical regions and in regions south of 32.5°S, covering about a fourth of the ocean surface area. Thus, the southern hemisphere high latitudes have a significant impact on future changes in ocean CO_2 uptake during this century in our model, but their influence diminishes thereafter. In contrast to the rest of the ocean, carbon uptake in the 1765–2100 period is enhanced in the North Atlantic in both stabilization simulations. The sign of global warming feedbacks at North Atlantic high latitudes is reversed after year 2100 in simulations where the Atlantic THC collapses completely (Fig. 8b).

4.4.2. Individual feedback mechanisms. We run the model in several configurations to quantify the various individual feedback mechanisms. The model simulations are listed and described in detail in Table 2. Results for WRE1000 and several periods are given in Table 3. As the ocean–atmosphere carbon cycle system is non-linear, the attribution of changes in ocean carbon uptake to different feedbacks is merely an approximation. We apply also an inorganic version of the model and performed some independent cross-checks to test the validity of this attribution.

4.4.2.1. Global. First we analyze global results. The "SST feedback" (simulation A–C; Table 3) dominates the reduction in global ocean carbon uptake in simulation WRE550 (Fig. 3c). This feedback reduces the CO_2 uptake by the ocean by about 16% in WRE550 by year 2500 (Fig. 9a). The "circulation feedback" (simulation D–E; Table 3) as well as the "marine biota feedback" (simulation E–B; Table 3) are significantly smaller on a global scale in WRE550. As they are of opposite sign, they nearly cancel each other. The contribution by the "dilution feedback" (simulation C–D; Table 3) is globally negligible. In simulation WRE1000 the complete collapse of NADW formation after year 2100 and the structurally different circulation pattern obtained thereafter (Fig. 4c) largely drive the reduction in CO_2 uptake by year 2500. However, the "SST feedback" is significant as well. The "SST feedback" governs the changes in ocean uptake until about year 2300 in WRE1000 (Fig. 3d), reducing the CO_2 uptake by 10% by the end of this century (Table 3). After year 2100, the "circulation feedback" significantly increases in strength as NADW formation collapses in WRE1000; by year 2500, the "circulation feedback" is responsible for a reduction in cumulative ocean carbon uptake of 21% compared to a 10% reduction owing to the "SST feedback"

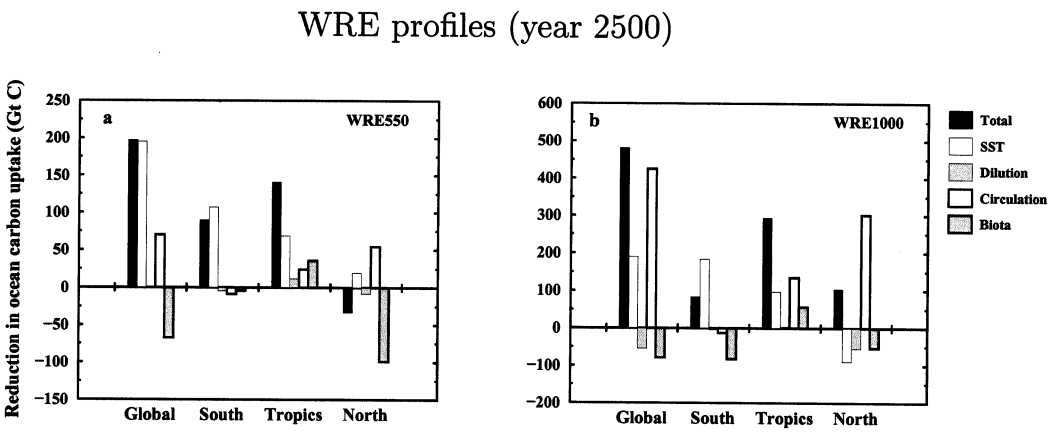

Fig. 9. Reduction in oceanic carbon uptake due to specified global warming feedbacks until year 2500. The total reduction is given for the standard model setup ($\Delta T_{2x} = 3.7°C$) and stabilization profiles WRE550 (a) and WRE1000 (b) compared to the constant-climate baseline ($\Delta T_{2x} = 0°C$). The contributions by different feedbacks are determined as described in Table 2 and listed in Table 3 (simulations A to H). Results are shown for different latitudinal regions (South: 70°S–32.5°S; Tropics: 32.5°S–32.5°N; North: 32.5°N–80°N). Positive values stand for a reduction and negative values for an increase in ocean CO_2 uptake.

(Fig. 9b). The "marine biota feedback" enhances oceanic CO_2 cuptake by 6% until year 2100 in simulation WRE1000, but its strength decreases thereafter.

The quality of the attribution of changes in ocean carbon uptake to different feedbacks is assessed. For this task, the model is run in different configurations as explained in detail in Table 2. The combined physical-chemical feedbacks in the standard model (simulation A–E; Table 3) agree well with a simulation using an abiotic version of the model (simulation J–K; Table 3). This suggests that the relatively small "marine biota feedback" and the sum of the "SST" plus "dilution" plus "circulation feedback" can be well quantified. Independent estimates of the "SST", "dilution" and "circulation feedback" show fairly good agreement with results obtained with the standard model setup (e.g., simulations L–E or A–N; Table 3). For WRE550 (not shown) the agreement is very good for all feedback mechanisms over the whole period from 1765–2500. However, for WRE1000, the agreement between independent estimates is getting worse beyond year 2100. For example, the reduction in ocean CO_2 uptake until year 2500 due to the "SST feedback" is estimated to be 9.4 and 13.3%, and the reduction by the "circulation feedback" is estimated to be 14.3 and 20.9% applying two different methods. Non-linearities in the carbon cycle and carbon chemistry hamper the exact quantification of individual feedback mechanisms, if ocean circulation changes and feedback strengths are becoming large as it is the case in WRE1000 after year 2100. In conclusion, the attribution to individual feedback mechanisms is reasonable, but uncertainties in their quantification exist.

4.4.2.2. Regional. Next, we quantify regionally the individual feedback mechanisms. In simulation WRE550 (Fig. 9a) until year 2500, the "SST feedback" reduces oceanic CO_2 uptake at all latitudes as expected from the warming of SST throughout the ocean. The impact of increasing SST on CO_2 uptake diminishes continuously from south to north. The "dilution feedback" is generally small. Until year 2100, the "marine biota feedback" is negative (enhancing ocean carbon uptake) at all latitudes (not shown). At year 2500, the "marine biota feedback" is negative at high latitudes and positive at low latitudes. The largely negative "marine biota feedback" in the North Atlantic is due to reduced NADW formation and an increase in the residence time of water in the euphotic zone, which allows a more efficient biological utilization of DIC. The "circulation feedback" reduces oceanic CO_2 uptake in the tropics and in the North Atlantic, where major circulation

changes occur, and slightly increases CO_2 uptake in the high latitudes of the southern hemisphere. The sign of the "marine biota feedback" remains unchanged in WRE1000 compared to WRE550 (Fig. 9b). The "marine biota feedback" is strongest at high latitudes of the southern hemisphere for WRE1000, in contrast to simulation WRE550. After a collapse of the THC the "SST feedback" turns negative at high northern latitudes owing to surface cooling in the North Atlantic (Schmittner and Stocker, 1999). Nevertheless, the "SST feedback" contributes significantly to the total reduction in ocean CO_2 uptake in WRE1000. The strength of the "circulation feedback" is largely increased at high latitudes in the northern hemisphere following the collapse in NADW formation after year 2300. In summary, individual feedback mechanisms and the sum of all feedback mechanisms on CO_2 uptake by the ocean exhibit strong regional variations.

4.4.2.3. "Biota-DIC" versus "biota-ALK feedback". We further investigate the "marine biota feedback" in more detail (Table 4). The "marine biota feedback" in our model is largely dictated by the slow-down in ocean circulation. The changes in the OM cycle and to a lesser extent in the $CaCO_3$ cycle tend to reduce surface DIC (Figs. 6b,e; scale at the right) and lead to a transient increase in CO_2 uptake ("biota-DIC feedback": simulation E–G; Table 4). On the other hand, the reduction in surface sALK ("biota-ALK feedback": simulation G–B; Table 4) decreases CO_2 uptake. In the standard model setup the "biota-DIC feedback" dominates the "biota-ALK feedback" and the net effect of the "marine biota feedback" is to slightly increase oceanic CO_2 uptake temporarily for all scenarios applied. In the long run, the "marine biota feedback" approaches zero. We determine the contributions of changes in the cycling of OM and in the cycling of $CaCO_3$ to the "biota-ALK feedback" and the "biota-DIC feedback" (Fig. 10). In the standard model setup, the "biota-OM/DIC feedback" largely exceeds the "biota-$CaCO_3$/DIC feedback", and the "biota-$CaCO_3$/ALK feedback" largely exceeds the opposite "biota-OM/ALK feedback" at any time. Thus, the "biota-DIC feedback" can be roughly attributed to changes in the OM cycle and the "biota-ALK feedback" to the changes in the $CaCO_3$ cycle.

4.4.2.4. Sensitivity of the "marine biota feedback" to model parameters. Next, we test the sensitivity of the "marine biota feedback" to various model parameters. We varied physical and biogeochemical parameters of the standard model setup in the range indicated in Table 1. We find that the net impact of the "marine biota feedback" by year 2500 is to increase ocean CO_2 uptake in

Table 4. *Reduction in ocean carbon uptake by different marine biota feedbacks and for different implementations of the marine biota for the WRE1000 CO_2 stabilization profile*

Simulation	Model setup	1980–1989	1765–2100	1765–2500
Estimated reduction in ocean uptake by differentiation of biota feedbacks (%)				
E–G	biota-DIC	−6.1	−8.0	−11.3
E–F	biota-$CaCO_3$/DIC	−0.5	−0.6	−2.7
F–G	biota-OM/DIC	−5.6	−7.4	−8.6
G–B	biota-ALK	1.4	2.1	7.5
G–H	biota-$CaCO_3$/ALK	1.9	2.9	8.1
H–B	biota-OM/ALK	−0.5	−0.8	−0.7
(E–F) + (G–H)	$CaCO_3$ cycle	1.4	2.3	5.4
(F–G) + (H–B)	OM cycle	−6.1	−8.2	−9.3
Reduction in ocean uptake for different implementations of the marine biota (%)				
(A–B) − (G–H) − (E–F)	no $CaCO_3$ feedback	4.2	5.6	18.4
A–I	constant export production	4.2	5.0	20.6
A–B	standard prognostic version	5.6	7.9	23.8
A–E	no biota feedback	10.3	13.8	27.6
(A–F) + (G–H)	no OM feedback	11.7	16.1	33.0

See Table 2 for detailed information about the model simulations.

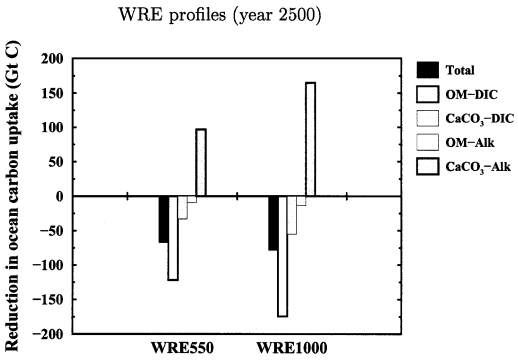

Fig. 10. Reduction in global oceanic carbon uptake due to the "marine biota feedback" and its different contributors until year 2500. The contributions by different feedbacks are determined as described in Table 2 and as listed in Table 4. All results are given for simulations with $\Delta T_{2x} = 3.7°C$ and CO_2 stabilization profiles WRE550 and WRE1000. Positive values stand for a reduction and negative values for an increase in ocean CO_2 uptake.

all global warming simulations, unless a relatively high value for the maximum production ratio of $CaCO_3$ to OM is used (prescribed). Then, the "marine biota feedback" approaches 0. In the latter case, however, surface DIC and ALK are too low at steady state compared to data. The largest "marine biota feedback" is modeled for low values of the vertical eddy diffusivity. Overall, the applied variations in model parameters lead to a range of 0 to +8% for the effect of the "marine biota feedback" on the uptake of CO_2 by the ocean by year 2500.

4.4.3. Alternative model implementations of the marine biota. In the standard model setup, export production of OM and $CaCO_3$ is described as a function of the availability of the macro-nutrient PO_4. Rate constants are diagnosed from the steady state PO_4 distribution. However, changes in CO_2, pH, and other environmental variables may affect ecosystem structure and the quality and quantity of exported material in various and unexpected ways. We have changed fundamental relationships in the marine biosphere model. The purpose is to explore, at least to some degree and from a geochemical point of view, the sensitivity of the reduction in oceanic carbon uptake to marine ecosystem changes.

In a first sensitivity simulation, we assume that export is driven by external factors such as light or aeolian iron input that remain constant in time. The biological export fluxes of OM and $CaCO_3$ are kept at their preindustrial values except when the euphotic zone PO_4 concentrations approach zero (simulation I, "constant export"; Table 3). Such an assumption yields lower estimates for the reduction in oceanic CO_2 uptake (simulation A–I; Table 4) than the standard model (simulation A–B; Table 4).

Next, we analyze a situation where marine ecosystems shift towards high abundance of $CaCO_3$ producers. A hypothetical "no OM feedback" case is constructed (Table 4), where only the biological feedbacks related to the $CaCO_3$ cycle and the abiotic feedbacks ("biota-$CaCO_3$/ALK", "biota-$CaCO_3$/DIC", "circulation", "dilution" and "SST feedback") are considered and where the biological feedbacks related to the OM cycle ("biota-OM/DIC" and "biota-OM/ALK feedback") are excluded. This yields upper estimates for the reduction in oceanic CO_2 uptake. Albeit possible, this scenario is inconsistent with recent work that suggests a reduction in calcification in response to increased CO_2 (Riebesell et al., 2000).

Then, we consider the possibility that the relative importance of $CaCO_3$ producers is reduced in the future by constructing a hypothetical "no $CaCO_3$ feedback" (Table 4). We do this by excluding the "biota-$CaCO_3$/DIC" and the "biota-$CaCO_3$/ALK feedback" in the model simulations. This yields a lower estimate for the reduction in oceanic CO_2 uptake.

In summary, the different implementations of the marine biosphere in our climate model yield ranges for the reduction in CO_2 uptake under WRE1000 (Table 4) of 5 to 16% and of 18 to 33% for the 1765–2100 and 1765–2500 periods, respectively.

4.5. Changes in marine oxygen inventory and implications for the interpretation of atmospheric O_2/N_2 measurements

Atmospheric measurements of the O_2/N_2 ratio have recently been used to determine the strength of oceanic and terrestrial sources and sinks of carbon (Keeling and Shertz, 1992; Keeling et al., 1996; Battle et al., 2000). The method is based on the assumption that changes in the atmospheric

O_2/N_2 ratio are only related to changes in terrestrial carbon storage and fossil fuel burning. A transient change in the oceanic O_2 inventory would cause a change in the atmospheric O_2/N_2 ratio, which would be erroneously attributed to a change in terrestrial carbon storage. We find that global warming–marine carbon cycle feedbacks significantly reduce the oceanic O_2 inventory. This is consistent with results reported by Sarmiento et al. (1998) and by Matear et al. (2000).

The oceanic and atmospheric O_2 inventories are coupled through gas exchange. O_2 is produced during photosynthesis in the ocean surface layer from where it is either lost to the atmosphere or transported to depth. The deep O_2 concentration and the oceanic O_2 inventory is determined by the balance between supply of O_2 from the surface and consumption by remineralization of OM at depth. At steady state, production at surface, transport to depth, and consumption are balanced, and the global air–sea flux is zero. The oceanic O_2 inventory in an isolated atmosphere–ocean system is constant, if O_2 consumption equals production. This is the case if organic carbon pools, here namely DOC_l, remain constant. A decrease in oceanic O_2 inventory corresponds then to an increase in atmospheric O_2. The oceanic O_2 inventory can be altered through changes in the marine biological cycling of OM or through changes in the O_2 solubility by changing SST and sea-surface salinities.

In "Preliminary Marker Scenario" A1, the ocean mean O_2 concentration is reduced by about 3 mmol m^{-3} up to year 1990 and by another 9 mmol m^{-3} from 1990 to 2100 These changes correspond to a reduction in global ocean inventory of $4 \cdot 10^{15}$ and $12 \cdot 10^{15}$ moles O_2, respectively. These inventory changes are comparable to results obtained with the GFDL OGCM by Sarmiento et al. (1998). Modeled changes in the DOC_l inventory are small. The oceanic O_2 loss in our model averages $5.2 \cdot 10^{13}$ mol yr^{-1} for 1980–1989 and $5.0 \cdot 10^{13}$ mol yr^{-1} for 1990–1999. To assess the implications for atmospheric O_2/N_2, we neglect thermally driven changes in atmospheric and oceanic N_2 inventories and use a stoichiometric factor of 1.1 between O_2 production and carbon storage in the terrestrial biosphere. Then, our results imply that the classical attribution of terrestrial and oceanic carbon sinks from O_2/N_2 measurements (Keeling and Shertz, 1992; Keeling et al., 1996; Battle et al., 2000) overestimates terrestrial carbon storage by about 0.6 GtC yr^{-1} during the decades from 1980–1989 ($5.2 \cdot 10^{13}/1.1$ molC $yr^{-1} = 0.57$ GtC yr^{-1}) and 1990–1999 ($5.0 \cdot 10^{13}/1.1$ molC $yr^{-1} = 0.55$ GtC yr^{-1}), and underestimates oceanic storage by the same amount.

We tentatively attribute the reduction in O_2 inventory to different mechanisms. We prescribed SST from global warming simulations to calculate the solubility of O_2, while running the model in the constant-climate baseline setup ($\Delta T_{2x} = 0°C$). About 27% of the total reduction up to 1990 can be attributed to the changes in O_2 solubility only, the rest stems from the combined effect of ocean circulation changes and changes in OM cycling. At year 2100, about 35% of the reduction is due to solubility changes only. For scenario A1 almost 80% of the reduction in the oceanic O_2 inventory at year 2100 are located north of 47.5°S, the northern boundary of the Southern Ocean in the model. We note that Matear et al. (2000) find the largest changes in O_2 uptake in the Southern Ocean. About 2/3 of the changes occur in ocean regions below 1000 m, mainly located in the Atlantic ocean.

5. Discussion

Ocean carbon uptake is reduced in global warming simulations compared to simulations assuming constant climate by 7 to 10% up to year 2100 for a wide range of future CO_2 and GHG emissions. This result is consistent with previous model studies that find reductions in the range of 4 to 28% during the 21st century (Maier-Reimer et al., 1996; Sarmiento and Le Quéré, 1996; Sarmiento et al., 1998; Joos et al., 1999; Matear and Hirst, 1999). The reduction in global ocean carbon uptake is 48 GtC until year 2100 for the stabilization profile WRE1000 in our model. This is consistent with the 56 GtC found by Matear and Hirst (1999), nearly double the 25 GtC found by Maier-Reimer et al. (1996) until 2100, and three times the 16 GtC reported by Sarmiento et al. (1998) until 2065, all using OGCMs. We note that these studies are not directly comparable as the investigated periods and the applied forcings differ between them.

The modeled reduction in carbon uptake differs regionally between the various modeling studies.

Climate change simulations with different OGCMs yield very different sensitivities of the Southern Ocean circulation to global warming. Sarmiento et al. (1998) and Matear and Hirst (1999) report significantly increased stratification of the upper water column in the Southern Ocean, leading to a decrease in vertical mixing along isopycnals and a decrease in convective overturning. Matear and Hirst (1999), applying a sophisticated subgrid-scale mixing parameterization (Gent et al., 1995), find that deep convection even stops in the Antarctic region. In contrast, Maier-Reimer et al. (1996) find only modest circulation changes in the Southern Ocean in their global warming simulations. Similarly ocean circulation changes in the Southern Ocean are modest in our model simulations (Schmittner and Stocker, 1999). The simulated reduction in oceanic CO_2 uptake by year 2100 is of similar magnitude in the Southern Ocean and in low-latitude regions (32.5°S–32.5°N) in our model. On longer timescales, the low latitudes' influence increases steadily. Results for simulations from the GFDL OGCM (Sarmiento and Le Quéré, 1996; Sarmiento et al., 1998) point to the Southern Ocean as the region mainly responsible for the reduction in ocean CO_2 uptake by global warming feedbacks until 2065. Both, the GFDL and our model overestimate the observed uptake of bomb-produced radiocarbon (Stocker et al., 1994; Toggweiler et al., 1989) and of anthropogenic carbon (Gruber, 1998) in the Southern Ocean. The coarse spatial resolution and the limited representation of Southern Ocean processes in our model (Knutti et al., 2000) and the weaker than observed stratification in the GFDL OGCM might contribute to the differences in results. Recent modeling intercomparison studies consistently show that results of comprehensive OGCMs differ most in the Southern Ocean region (Sarmiento et al., 2000; Orr et al., 2001; Dutay et al., 2001).

Until year 2100, the simulated carbon uptake in the North Atlantic is higher for simulations with global warming than for simulations without it in our model. This contrasts with OGCM results reported by Maier-Reimer et al. (1996). These authors found that CO_2 uptake is reduced in the North Atlantic ocean by year 2100 owing to GHG forcing and the subsequent warming. In their simulation, NADW formation is only slightly reduced from 25 Sv to 21 Sv, whereas in our model simulations, NADW formation is reduced by 40% to 60% until 2100. Such a reduction might be on the high end, as potentially THC-stabilizing mechanisms (Stocker et al., 2001) such as an enhanced water vapor export out of the Atlantic (Latif et al., 2000; Schmittner et al., 2000) are not included. These comparisons suggest that global warming–marine carbon cycle feedbacks are not well understood on a regional scale.

The reduction in oceanic CO_2 uptake by sea surface warming ("SST feedback") is consistently estimated in different studies. Sarmiento et al. (1998) and Matear and Hirst (1999) found a reduction in ocean uptake due to decreased CO_2 solubility of 14% (56 GtC) and 13% (48 GtC), similar to the reduction of around 10% (58 GtC) found in this study. All studies find that the reduction in ocean circulation leads to a reduced uptake, and suggest that the changes in the marine biological cycles lead to a transient increase in ocean uptake. The strength of the reduction caused by the combination of the slowdown of surface-to-deep transport and changes in the marine biological cycles ("circulation" plus "marine biota feedback") is similar in the study by Matear and Hirst (1999) (2% reduction in uptake) and in this study (1% increase in uptake). In contrast, Sarmiento et al. (1998) find a 10% increase in CO_2 uptake by these two mechanisms. Sarmiento et al. (1998) find much larger individual contributions on carbon uptake from circulation changes (reduction of 17%) and changes in the marine biological cycles (increase of 27%) than Matear and Hirst (1999) (11% reduction; 9% increase) and this study (5% reduction; 6% increase). The difference is largely related to the Southern Ocean, where the GFDL model shows large changes in stratification and circulation under projected global warming. Furthermore, Sarmiento et al. (1998) prescribe export production of organic carbon and $CaCO_3$ to be constant in their simulations.

We find a small 4% increase in atmospheric CO_2 due to the reduction in the CO_2 uptake by the ocean associated with the warming scenarios. However, we did not account for global warming-terrestrial carbon cycle feedbacks in our model simulations. Recent modeling studies investigating oceanic and terrestrial global warming feedbacks (Cox et al., 2000; Lenton, 2000), find a significantly reduced terrestrial carbon uptake under global warming and their results suggest that the global

warming-terrestrial carbon cycle feedbacks largely exceed the global warming–marine carbon cycle feedbacks.

Observations of atmospheric O_2/N_2 are used to estimate the magnitude of the terrestrial and oceanic carbon sinks and sources under the assumption that changes in O_2/N_2 are only caused by fossil fuel burning and terrestrial carbon storage on a multi-annual timescale (Keeling and Shertz, 1992; Keeling et al., 1996; Battle et al., 2000). However, global warming feedbacks have the potential to significantly shift the partitioning of O_2 between the ocean and the atmosphere (Sarmiento et al., 1998; Matear et al., 2000). The oceanic inventory is reduced and the atmospheric inventory is increased in our global warming simulations. This shift is predominantly driven by the combined effect of ocean circulation changes and changes in OM cycling that lead to an enhanced nutrient storage and a reduced O_2 storage in the deep ocean. Surface warming also contributes significantly to the reduction. Our model results suggest that the terrestrial CO_2 sink as deduced from O_2/N_2 observations is overestimated and the oceanic sink underestimated by about 0.6 GtC yr^{-1} for the 1980–1989 and 1990–1999 periods, if marine O_2 inventory changes are not considered. This implies that information in addition to atmospheric O_2/N_2 measurements is required to take into account possible oceanic O_2 inventory changes and to correctly partition between the terrestrial and oceanic carbon sinks. An alternative option to models, would be to run ocean surveys on a regular basis to estimate the trend in the oceanic O_2 inventory from observations.

6. Conclusions

Our results suggest that global warming leads to large-scale changes in the marine environment in physical, chemical, and biological parameters. Circulation changes and NADW formation in particular decreases in all scenarios and CO_2 stabilization profiles considered. The circulation changes are driven by increasing ocean temperatures and an enforced hydrological cycle that leads to a freshening of high-latitude surface waters. The biogeochemical cycles and the distribution of nutrients, DIC, ALK and O_2 are markedly altered. In general, nutrient concentrations are lowered in the upper ocean and increased in the deep ocean. Relatively nutrient-poor waters are replaced by nutrient-rich waters in the deep North Atlantic. The production and export of OM and $CaCO_3$ decreases under global warming. The projected changes could potentially have significant implications for the marine ecosystem structure and the marine food web.

The oceanic O_2 inventory decreases and the atmospheric inventory increases in our global warming simulations. This suggests that terrestrial carbon uptake may be overestimated and oceanic uptake underestimated by a few tenths of a GtC in the budgets of anthropogenic CO_2 recently published in the IPCC Third Assessment Report (Prentice et al., 2001). We suggest that the oceanic distribution of oxygen should be regularly monitored to reduce uncertainties in the CO_2 budget.

Large-scale changes in the ocean biogeochemical cycles lead to a reduction in the uptake of atmospheric CO_2 by the ocean in simulations with global warming relative to those without it. By year 2100, the impact of this reduction in CO_2 uptake on DIC is projected to extend to the bottom in the Southern Ocean and in the North Atlantic, but to be restricted to the upper 1000 m in the Pacific and Indian Oceans.

The reduction in ocean uptake due to increasing temperatures (reduced CO_2 solubility) is the most important feedback mechanism associated with the uptake of atmospheric CO_2 by the ocean in our model, except when NADW formation stops. This "SST feedback" is plausible based on theoretical ground and consistently found in all global warming modeling studies investigating ocean CO_2 uptake (Klepper and de Haan, 1995; Maier-Reimer et al., 1996; Sarmiento and Le Quéré, 1996; Sarmiento et al., 1998; Joos et al., 1999; Matear and Hirst, 1999). Recent analyses of observations confirm that the ocean heat content has significantly increased in the past decades (Levitus et al., 2000).

The magnitude, at global and regional levels, of the feedback mechanisms associated with a reduction in the ocean thermohaline circulation and changes in the biological cycles are less certain and significant discrepancies are found between individual modeling studies (Cubasch et al., 2001).

Changes in the marine biological cycles lead to a transient increase in ocean CO_2 uptake in the

standard model setup, although export production of OM and $CaCO_3$ is reduced. Obviously, the picture of a "biological pump", which removes carbon continuously from the atmosphere in proportion to the export flux of biological material out of the surface ocean, is incorrect.

The net effect of changes in the marine biological cycles on CO_2 uptake is the sum of two potentially large but opposite mechanisms that are associated with changes in the cycling of OM and $CaCO_3$, respectively. In our model, the two mechanisms tend to cancel each other. However, changes in marine ecosystem structure are difficult to project and the changes may be significantly different from those modeled here.

A sensitivity study applying different formulations for the marine biosphere and varying model parameters yields that the reduction in ocean uptake until 2500 for the CO_2 stabilization profile WRE1000 varies between 18% and 33% in simulations with global warming relative to simulations without it. Our results suggest that only extreme changes in marine ecosystem structure may lead to a substantially different "marine biota-feedback" of oceanic CO_2 uptake than estimated by our standard model.

The difference in projected atmospheric CO_2 is around 4% at year 2100 between simulations with global warming and simulations without it for the range of IPCC (SRES and IS92) scenarios considered; the difference in ocean uptake is around 10% until 2100. The deduced emissions from the CO_2 stabilization profiles are larger in the constant-climate simulations than in the global warming simulations. The difference in cumulated emissions at year 2100 reaches 41 GtC for WRE550 and 48 GtC for WRE1000. This corresponds to a reduction of nearly 3% in both WRE cases owing to global warming.

Atmospheric CO_2 at year 2100 is projected between 471 ppm and 1071 ppm for the IPCC SRES scenarios. All SRES scenarios are non-climate policy intervention scenarios. Stabilization of atmospheric CO_2 and radiative forcing until the end of this century is only realized for the SRES scenario with the lowest cumulative carbon emissions.

7. Acknowledgments

We thank N. Gruber for providing data-based anthropogenic CO_2 estimates for the Atlantic Ocean. We enjoyed discussions with R. Knutti and A. Schmittner. Constructive comments by N. Gruber and an anonymous reviewer are acknowledged. This work is supported by the Swiss National Science Foundation and the Swiss Federal Office of Science and Education through the EC-projects GOSAC and MilEClim. GOSAC contributes to the IGBP/GAIM Ocean Carbon-Cycle Model Intercomparison Project (OCMIP) activity.

REFERENCES

Battle, M., M. L. Bender, P. P. Tans, J. M. C. White, J. T. Ellis, T. Conway and R. J. Francey, 2000. Global carbon sinks and their variability inferred from atmospheric CO_2 and ^{13}C. *Science* **287**, 2467–2470.

Bishop, J. K. B. 1989. Regional extremes in particulate matter composition and flux: effects on the chemistry of the ocean interior. In: *Productivity of the ocean: present and past*. eds: W. H. Berger, V. S. Smetacek and G. Wefer. New York, John Wiley, pp. 117–137.

Broecker, W. S., T.-H. Peng, G. Östlund and M. Stuiver, 1985. The distribution of bomb radiocarbon in the ocean. *J. Geophys. Res.* **90**, 6953–6970.

Cao, M. and F. I. Woodward, 1998. Dynamic response of terrestrial ecosystem carbon cycling to global climate change. *Nature* **393**, 249–252.

Conkright, M. E., S. Levitus and T. P. Boyer, 1994. *World ocean atlas 1994*, vol. 1: *Nutrients*. Washington, DC: US Department of Commerce, NOAA, NESDIS, 150 pp.

Cox, P. M., R. A. Betts, C. D. Jones, S. A. Spall and I. J. Totterdell, 2000. Will carbon-cycle feedbacks accelerate global warming in the 21st century? *Nature* **408**, 184–187.

Cubasch, U., G. Meehl, G. Boer, R. Stouffer, M. Dix, A. Noda, C. Senior, S. Raper and K. S. Yap, 2001. Projections of future climate change. In: *Third assessment report of climate change*. ed: J. T. Houghton. Cambridge University Press, New York, in press.

Drange, H. 1994. *An isopycnic coordinate carbon cycle model for the North Atlantic; and the possibility of disposing of fossil fuel CO_2 in the ocean.* PhD thesis, Department of Mathematics, University of Bergen, Norway.

Dutay, J.-C., J. L. Bullister, S. C. Doney, J. C. Orr, R. Najjar, K. Caldeira, J.-M. Campin, H. Drange, M. Follows, Y. Gao, N. Gruber, M. W. Hecht, A. Ishida, F. Joos, K. Lindsay, G. Madec, E. Maier-Reimer, J. C. Marshall, R. J. Matear, P. Monfray, G.-K. Plattner, J. Sarmiento, R. Schlitzer, R. Slater,

I. J. Totterdell, M.-F. Weirig, Y. Yamanaka and A. Yool, 2001. Evaluation of ocean model ventilation with CFC-11: comparison of 13 global ocean models. *Ocean Modelling*, in press.

Friedlingstein, P., L. Bopp, P. Ciais, J.-L. Dufresne, L. Fairhead, H. Le Treut, P. Monfray and J. Orr, 2001. Positive feedback between future climate change and the carbon cycle. *Geophys. Res. Lett*., in press.

Fuglestvedt, J. and T. Berntsen, 1999. A simple model for scenario studies of changes in global climate. *Working Paper, 1999:2*. Center for International Climate and Environmental Research, Oslo, Norway.

Ganachaud, A. and C. Wunsch, 2000. Improved estimates od global ocean circulation, heat transport and mixing from hydrographic data. *Nature* **408**, 453–457.

Gent, P. R., J. Willebrand, T. J. McDougall and J. C. McWilliams, 1995. Parameterizing eddy-induced tracer transports in ocean circulation models. *J. Phys. Oceanogr*. **25**, 463–474.

Gordon, A. L. 1986. Interocean exchange of thermocline water. *J. Geophys. Res*. **91**, 5037–5046.

Gruber, N., J. L. Sarmiento and T. F. Stocker, 1996. An improved method for detecting anthropogenic CO_2 in the oceans. *Global Biogeochem. Cyc*. **10**, 809–837.

Gruber, N. 1998. Anthropogenic CO_2 in the Atlantic Ocean. *Global Biogeochem. Cyc*. **12**, 165–192.

Gruber, N. and C. D. Keeling, 2001. An improved estimate of the isotopic air–sea disequilibrium of CO_2: implications for the oceanic uptake of anthropogenic CO_2. *Geophys. Res. Lett*. **28**, 555–558.

Gruber, N. and J. L. Sarmiento, 2001. *The sea — biological/physical interactions. Large-scale biogeochemical/physical interactions in elemental cycles*. John Wiley, pp. 1–64.

Han, Y. J. and S. W. Lee, 1983. An analysis of monthly mean windstress over the global ocean. *Mon. Weather Rev*. **111**, 1554–1566.

Harvey, L. D. D., J. Gregory, M. Hoffert, A. Jain, M. Lal, R. Leemans, S. Raper, T. Wigley and J. de Wolde, 1997. IPCC Technical Paper II. *An introduction to simple climate models used in the IPCC second assessment report*. Intergovernmental Panel on Climate Change, 47 pp.

IPCC, 1996. *Climate change 1995. The science of climate change*. Intergovernmental Panel on Climate Change, Cambridge University Press, 572 pp.

IPCC, 2001. *Third assessment report of climate change*. Intergovernmental Panel on Climate Change, Cambridge University Press, in press.

Joos, F., M. Bruno, R. Fink, U. Siegenthaler, T. F. Stocker, C. Le Quéré and J. Sarmiento, 1996. An efficient and accurate representation of complex oceanic and biospheric models of anthropogenic carbon uptake. *Tellus* **48B**, 397–417.

Joos, F., G.-K. Plattner, T. F. Stocker, O. Marchal and A. Schmittner, 1999. Global warming and marine carbon cycle feedbacks on future atmospheric CO_2. *Science* **284**, 464–467.

Keeling, R. F. and S. R. Shertz, 1992. Seasonal and interannual variations in atmospheric oxygen and implications for the global carbon cycle. *Nature* **358**, 723–727.

Keeling, R. F., S. C. Piper and M. Heimann, 1996. Global and hemispheric CO_2 sinks deduced from changes in atmospheric O_2 concentrations. *Nature* **381**, 218–221.

Kicklighter, D. W., M. Bruno, S. Doenges, G. Esser, M. Heimann, J. Helfrich, F. Ift, F. Joos, J. Kaduk, G. H. Kohlmaier, A. C. McGuire, J. M. Melillo, R. Meyer, B. Moore III, A. Nadler, I. C. Prentice, W. Sauf, A. L. Schloss, S. Sitch, U. Wittenberg and G. Wuerth, 1999. A first order analysis of the potential role of CO_2 fertilization to affect the global carbon budget: a comparison of four terrestrial biosphere models. *Tellus* **51B**, 343–366.

Klepper, O. and B. J. de Haan, 1995. A sensitivity study of the effect of global change on ocean carbon uptake. *Tellus* **47B**, 490–500.

Knutti, R., T. F. Stocker and D. G. Wright, 2000. The effects of sub-grid-scale parameterizations in a zonally averaged ocean model. *J. Phys. Oceanogr*. **30**, 2738–2752.

Latif, M., E. Roeckner, U. Mikolajewicz and R. Voss, 2000. Tropical stabilization of the thermohaline circulation in a greenhouse warming simulation. *J. Clim*. **13**, 1809–1813.

Legget, J., W. J. Pepper and R. J. Swart, 1992. *Climate change 1992. The Supplementary Report to the IPCC Scientific Assessment*. Emissions Scenarios for IPCC: An Update. Cambridge University Press, pp. 69–95.

Lenton, T. M. 2000. Land and ocean carbon cycle feedback effects on global warming in a simple Earth system model. *Tellus* **52B**, 1159–1188.

Levitus, S. 1982. *Climatological atlas of the world ocean*. Washington, DC: US Govt. Print. Office, NOAA Prof. Pap. 13, 173 pp.

Levitus, S., R. Burgett and T. P. Boyer, 1994. *World ocean atlas 1994*, vol. 3: *Salinity*. Washington DC: US Department of Commerce, NOAA, NESDIS, 99 pp.

Levitus, S. and T. P. Boyer, 1994. *World ocean atlas 1994*, vol. 4: *Temperature*. Washington DC: US Department of Commerce, NOAA, NESDIS, 117 pp.

Levitus, S., J. I. Antonov, T. P. Boyer and C. Stephens, 2000. Warming of the World Ocean. *Science* **287**, 2225–2229.

Maier-Reimer, E. and K. Hasselmann, 1987. Transport and storage of CO_2 in the ocean — an inorganic ocean-circulation carbon cycle model. *Clim. Dyn*. **2**, 63–90.

Maier-Reimer, E., U. Mikolajewicz and A. Winguth, 1996. Future ocean uptake of CO_2: interaction between ocean circulation and biology. *Clim. Dyn*. **12**, 711–721.

Manabe, S. and R. J. Stouffer, 1993. Century-scale effects of increased atmospheric CO_2 on the ocean–atmosphere system. *Nature* **364**, 215–218.

Manabe, S. and R. J. Stouffer, 1994. Multiple-century response of a coupled ocean–atmosphere model to an

increase of atmospheric carbon dioxide. *J. Clim.* **7**, 5–23.

Marchal, O., T. F. Stocker and F. Joos, 1998a. A latitude-depth, circulation-biogeochemical ocean model for paleoclimate studies. Model development and sensitivities. *Tellus* **50B**, 290–316.

Marchal, O., T. F. Stocker and F. Joos, 1998b. Impact of oceanic reorganizations on the ocean carbon cycle and atmospheric carbon dioxide content. *Paleoceanogr.* **13**, 225–244.

Marchal, O., T. F. Stocker, F. Joos, A. Indermühle, T. Blunier and J. Tschumi, 1999a. Modelling the concentration of atmospheric CO_2 during the Younger Dryas climate event. *Clim. Dyn.* **15**, 341–354.

Marchal, O., T. F. Stocker and F. Joos, 1999b. Physical and biogeochemical responses to freshwater-induced thermohaline variability in a zonally averaged ocean model. In: *Mechanisms of global climate change at millennial time scales.* eds: P. U. Clark, R. S. Webb and L. D. Keigwin. *Geophysical Monograph* **112**, Am. Geophys. Union, Washington, DC, pp. 263–284.

Matear, R. J. and A. C. Hirst, 1999. Climate change feedback on the future oceanic CO_2 uptake. *Tellus* **51B**, 722–733.

Matear, R. J., A. C. Hirst and B. I. McNeil, 2000, Changes in dissolved oxygen in the Southern Ocean with climate change. *Geochem. Geophys. Geosyst* **1**, Paper number 2000GC000086.

Meyer, R., F. Joos, G. Esser, M. Heimann, G. Kohlmaier, W. Sauf and U. Wittenberg, 1999. The substitution of high-resolution terrestrial biosphere and carbon sequestration in response to changing CO_2 and climate. *Global Biogeochem. Cyc.* **13**, 785–802.

Murnane, R. J., J. L. Sarmiento and C. LeQuere, 1999. Spatial distribution of air–sea CO_2 fluxes and the interhemisperic transport of carbon by the oceans. *Global Biogeochem. Cyc.* **13**, 287–305.

Myhre, G., K. P. Highwood, E. J. Shine and F. Stordal, 1998. New estimates of radiative forcing due to well mixed greenhouse gases. *Geophys. Res. Lett.* **25**, 2715–1718.

Najjar, R. G., J. L. Sarmiento and J. R. Toggweiler, 1992. Downward transport and fate of organic matter in the ocean: Simulations with a general circulation model *Global Biogeochem. Cyc.* **6**, 45–76.

Nakićenović et al., 2000. *Special report on emission scenarios.* Intergovernmental Panel on Climate Change, Cambridge University Press, 599 pp.

Oeschger, H., U. Siegenthaler, U. Schotterer and A. Gugelmann, 1975. A box diffusion model to study the carbon dioxide exchange in nature. *Tellus* **27**, 168–192.

Orr, J. C., E. Maier-Reimer, U. Mikolajewicz, P. Monfray, J. L. Sarmiento, J. R. Toggweiler, N. K. Taylor, P. J., N. Gruber, C. L. Sabine, C. Le Quéré, R. M. Key and J. Boutin, 2001. Estimates of anthropogenic carbon uptake from four three-dimensional global ocean models. *Global Biogeochem. Cyc.* **15**, 43–60.

Prentice, I. C., G. Farquahr, M. Fasham, M. Goulden, M. Heimann, V. Jaramillo, H. Kheshgi, C. Le Quéré, R. Scholes and D. Wallace, 2001. The carbon cycle and atmospheric CO_2. In: *Third assessment report of climate change*, ed: J. T. Houghton. Cambridge University Press, New York, in press.

Revelle, R. and H. E. Suess, 1957. Carbon dioxide exchange between atmosphere and ocean and the question of an increase of atmospheric CO_2 during the past decades. *Tellus* **9**, 18–27.

Revelle, R. 1985. The scientific history of carbon dioxid. In: *The carbon cycle and atmospheric CO_2: natural variations archean to present*, eds: E. T. Sundquist and W. S. Broecker. *Geophysical Monograph* **32**, Am. Geophys. Union, Washington, DC, pp. 1–4.

Riebesell, U., I. Zondervan, B. Rost, P. D. Tortell, R. E. Zeebe and F. M. M. Morel, 2000. Reduced calcification of marine plankton in response to increased atmospheric CO_2. *Nature* **407**, 364–367.

Sabine, C. L., R. M. Key, C. Goyet, K. M. Johnson, F. J. Millero, A. Poisson, J. L. Sarmiento, D. W. R. Wallace and C. D. Winn, 1999. Anthropogenic CO_2 inventory of the Indian Ocean. *Global Biogeochem. Cyc.* **13**, 179–198.

Sarmiento, J. L. 1991. Oceanic uptake of anthropogenic CO_2: the major uncertainties. *Global Biogeochem. Cyc.* **5**, 309–313.

Sarmiento, J. L. and C. Le Quéré, 1996. Oceanic carbon dioxide in a model of century-scale global warming. *Science* **274**, 1346–1350.

Sarmiento, J. L., T. M. C. Hughes, R. J. Stouffer and S. Manabe, 1998. Simulated response of the ocean carbon cycle to anthropogenic climate warming. *Nature* **393**, 245–249.

Sarmiento, J. L., P. Monfray, E. Maier-Reimer, O. Aumont, R. Murnane and J. C. Orr, 2000. Sea–air CO_2 fluxes and carbon transport: a comparison of three ocean general circulation models. *Global Biogeochem. Cyc.* **14**, 1267–1281.

Schimel, D., D. Alves, I. G. Enting, M. Heimann, F. Joos, D. Raynaud and T. M. L. Wigley, 1996. CO_2 and the carbon cycle. In: *IPCC second scientific assessment of climate change*, ed: J. T. Houghton. Cambridge University Press, New York, pp. 76–86.

Schimel, D., M. Grubb, F. Joos, R. Kaufmann, R. Moos, W. Ogana, R. Richels and T. Wigley, 1997. IPCC Technical Paper III. *Stabilisation of atmospheric greenhouse gases: physical, biological and socio-economic implications.* Intergovernmental Panel on Climate Change, 48 pp.

Schmittner, A. and T. F. Stocker, 1999. The stability of the thermohaline circulation in global warming experiments. *J. Clim.* **12**, 1117–1133.

Schmittner, A., C. Appenzeller and T. F. Stocker, 2000. Enhanced Atlantic freshwater export during El Niño. *Geophys. Res. Let.* **27**, 1163–1166.

Schmitz, W. J. 1995. On the interbasin-scale thermohaline circulation. *Rev. Geophys.* **33**, 151–173.

Siegenthaler, U. and H. Oeschger, 1987. Biospheric CO_2 emissions during the past 200 years reconstructed by convolution of ice core data. *Tellus* **39B**, 140–154.

Siegenthaler, U. and F. Joos, 1992. Use of a simple model for studying oceanic tracer distributions and the global carbon cycle. *Tellus* **44B**, 186–207.

Stocker, T. F., D. G. Wright and L. A. Mysak, 1992. A zonally averaged, coupled ocean–atmosphere model for paleoclimate studies. *J. Clim.* **5**, 773–797.

Stocker, T. F., W. S. Broecker and D. G. Wright, 1994. Carbon uptake experiments with a zonally-averaged global ocean circulation model. *Tellus* **46B**, 103–122.

Stocker, T. F. and D. G. Wright, 1996. Rapid changes in ocean circulation and atmospheric radiocarbon. *Paleoceanogr.* **11**, 773–796.

Stocker, T. F. and A. Schmittner, 1997. Influence of CO_2 emission rates on the stability of the thermohaline circulation. *Nature* **388**, 862–865.

Stocker, T. F., R. Knutti and G.-K. Plattner, 2001. The future of the thermohaline circulation – a perspective. In: *Oceans and rapid past and future climate changes: north–south connections*, eds: D. Seidov, M. Maslin and B. J. Haupt. *Geophysical Monograph*, Am. Geophys. Union, Washington DC, in press.

Takahashi, T., W. S. Broecker, S. R. Werner and A. E. Bainbridge, 1980. Carbonate chemistry of the surface waters of the World Oceans, In: *Isotope marine chemistry*, eds: E. D. Goldberg, Y. Horibe and K. Saruhashi. Uchida Rokakuho Pub. Co. Ldt., pp. 291–326.

Takahashi, T., J. Olafsson, J. G. Goddard, D. W. Chipman and S. C. Sutherland, 1993. Seasonal variation of CO_2 and nutrients in the high-latitude surface oceans: a comparative study. *Global Biogeochem. Cyc.* **7**, 843–878.

Toggweiler, J. R., K. Dixon and K. Bryan, 1989. Simulation of radiocarbon in a coarse-resolution world ocean model, 2. Distributions of bomb-produced carbon 14. *J. Geophys. Res.* **94**, 8243–8264.

Wigley, T. M. L., A. K. Jain, F. Joos, B. S. Nyenzi and P. R. Shukla, 1997. IPCC Technical Paper IV. *Implications of proposed CO_2 emissions limitations*. Intergovernmental Panel on Climate Change, 41 pp.

Wright, D. G., C. B. Vreugdenhil and T. M. Hughes, 1995. Vorticity dynamics and zonally averaged ocean circulation models. *J. Phys. Oceanogr.* **25**, 2141–2154.